Improving Hydrogen Sensors for Diagnostics in Heavy Duty Fuel Cell Applications

by

Daniel Kenneth Zwart

B.A.Sc. (Hons., Mechanical Engineering), University of Waterloo, 2009

Thesis Submitted in Partial Fulfillment

of the Requirements for the Degree of

Master of Applied Science

in the

School of Mechatronic Systems Engineering

Faculty of Applied Sciences

© Daniel Kenneth Zwart 2014

SIMON FRASER UNIVERSITY

Summer 2014

Approval

Name:	**Daniel Kenneth Zwart**
Degree:	**Master of Applied Science**
Title of Thesis:	***Improving Hydrogen Sensors for Diagnostics in Heavy Duty Fuel Cell Applications***

Examining Committee:

Chair: Krishna Vijayaraghavan
Assistant Professor

Farid Golnaraghi
Senior Supervisor
Professor and Chair

Erik Kjeang
Supervisor
Assistant Professor

Jake DeVaal
External Examiner
Product Safety Manager, Systems Engineering Dept
Ballard Power Systems Inc.

Date Defended/Approved: June 02 2014

Partial Copyright Licence

SFU

Abstract

Ballard Power Systems is a leading company in the field of hydrogen fuel cell research and manufacture. Monitoring membrane deterioration through excessive crossover requires accurate hydrogen leak sensors within the vehicle safety systems. Hydrogen sensors are typically used to detect fuel crossover and external leaks in fuel cells. They are expensive and have typically exhibited short lifetimes. Two methods of lengthening the sensor life have been examined in this thesis. The first is physical filtering of poisoning agents. These components, particularly the siloxane compounds that are off-gassed from the silicone tubing, coalesce on the surface of the hydrogen sensor as silicates, reducing the sensor sensitivity. With these compounds mostly removed by the filters, the sensor life has been extended. While preventing degradation of the cathode exhaust sensor is the best approach, it was not wholly effective. Significant effort went into recalibrating the hydrogen sensor in situ, the second method. This methodology uses anode and cathode mass flow sensors in the fuel cell to automatically calibrate the hydrogen sensor as it degrades. The results from this approach were found to be promising, and we showed that the auto-calibration algorithm was robust enough to accept disturbances in system inputs.

Keywords: fuel cell; hydrogen sensor degradation; hydrogen sensor filters; calibration; siloxane; in-situ calibration

I dedicate this thesis to my future wife (unknown) and children, who had to wait so patiently while I was ignoring them to work on my thesis.
I also dedicate this thesis to my brother Andrew. At least one of us finished.
And finally, I would like to dedicate this thesis to my parents, who ensured I didn't quit.

Acknowledgements

Table of Contents

List of Tables

List of Figures

List of Acronyms and Glossary

ANFIS	Adaptive Neural Fuzzy Inference System
ANN	Adaptive Neural Network
APC	Automotive Partnership Canada
Ballard	Ballard Power Systems Inc.
CL	Catalyst Layer
CVM	Cell Voltage Monitoring
DC	Direct Current
DI	De-Ionized
dP	Differential Pressure
EDS	Energy Dispersive x-ray Spectroscopy
EPTFE	Expanded Polytetrafluoroethylene–a porous flexible material-Teflon
Expanded Single Fuel Cell	A single fuel cell consists of the membrane electrode assembly and two flow field plates
HD6	FCvelocity$^{®}$-HD6, Ballard's 6th generation heavy duty fuel cell module
Flow Field Plates	Gases (hydrogen and air) are supplied to the electrodes of the membrane electrode assembly through channels formed in flow field plates
Fuel (Hydrogen)	Hydrogen flows through channels in flow field plates to the anode where the platinum catalyst promotes its separation into protons and electrons.
Fuel Cell Module	The fuel cell module includes the fuel cell stack, electrical interface, air humidifier, flow control mechanism, and more
Fuel Cell Stack	Individual fuel cells are combined to form a fuel cell stack. Increasing the number of cells in a stack increases the voltage, while increasing the surface area of the cells increases the current
GLY	Glycol
H2	Hydrogen
HD / P	Heavy Duty. The class of vehicle designating buses. Ie. HD6, Phase 5 (P5)
HMDSO	Hexamethyldisiloxane
HRB	Hydrogen Recirculation Blower
IN	Inlet
LFL/LEL	Lower Flammability Limit / Lower Explosive Limit
Load	Current draw on the fuel cell

Membrane Electrode Assembly (MEA)	Each membrane electrode assembly consists of two electrodes (anode and cathode) with a very thin layer of catalyst and gas diffusion layer on either side
MFC	Mass Flow Controller
MK1100	Fuel cell type used in HD6 fuel cell modules
NSERC CRD	Natural Sciences and Engineering Research Council of Canada (NSERC) Collaborative Research and Development
Oxidant (air)	Air flows through the channels in flow field plates to the cathode. The hydrogen protons that migrate through the proton exchange membrane combine with oxygen in air and electrons returning from the external circuit to form pure water and heat.
P & ID	Process and Instrumentation Diagram
PCV	Pressure Control Valve
PEM	Proton Exchange Membrane / Polymer Electrolyte Membrane, the membrane used in one type of fuel cell, usually with hydrogen as a fuel. It is also a name used for fuel cells that use this membrane.
PFSA	Perfluorosulfonic acid, the electrolytic membrane material used
PMP	Pump
PPE	Personal Protective Equipment
RKI	Riken Keiki Instruments Inc., hydrogen sensor supplier
sccm	Standard cubic centimetres per minute
SEM	scanning electron microscope
Sensor degradation	The process of siloxanes oxidizing on the surface of the sensor to form silicate, reducing the ability of hydrogen to reach the sensor and reducing the signal level
SEP	Water separator
SiO2	Silica
SLPM	Standard Litres per Minute – normalized to 0 °C and 1 atmosphere
SOV	Solenoid operated purge valve

Nomenclature

$\dot{n}_{a,in}$	Hydrogen inlet flow rate
$\dot{n}_{cons}$	Hydrogen consumption rate in the production of electricity
$\dot{n}_{l,int}$	Internal hydrogen leak rate
$\dot{n}_{l,ext}$	External hydrogen leak rate
$\dot{n}_{a,out}$	Hydrogen purge rate to the cathode exhaust
$\dot{n}_{a,perm}$	Hydrogen crossover to cathode
$\dot{n}_{c,in}$	Air inlet flow rate
$\dot{n}_{c,out}$	Air inlet flow rate
$\dot{n}_{l,out}$	Rate of internal hydrogen leak exiting cathode exhaust
$P_{a,in}$	Pressure – anode inlet
$P_{a,out}$	Pressure –anode outlet
$P_{c,in}$	Pressure –cathode inlet
$P_{c,out}$	Pressure –cathode outlet
C_{H_2}	Cathode exhaust hydrogen concentration reading
V, V_a, V_c	Back pressure valves

1. Fuel Cell Bus Safety

1.1. Introduction

Over the past decade governments and transit agencies world-wide have been promoting measures to reduce airborne emissions and greenhouse gases from vehicles. Zero emission vehicles can make an important contribution to this effort. Ballard Power Systems, in collaboration with coach supplier New Flyer Industries from Winnipeg, has built a fleet of 20 hydrogen fuel cell powered hybrid buses. These were placed in regular service by BC Transit in Whistler for the 2010 Winter Olympics and subsequent continuing service. Powered by Ballard's 6th generation FCvelocity®-HD6 (HD6) Modules, these buses utilize two Mk1100 Proton Exchange Membrane (PEM) stacks. Lithium ion batteries are used for energy storage and acceleration, making these buses "hybrids," and are used in conjunction with the fuel cells. They allow the fuel cells to continuously produce power at a rate to optimize the efficiency and performance of the fuel cells. The batteries store the fuel cell energy during times when it is not needed as well storing the energy from regenerative braking. They give bursts of power for short duration acceleration. This fleet constitutes the world's largest fuel cell bus fleet, and represents an opportunity for Canada to both showcase and to develop this world-class product.

While significant progress towards fully commercial fuel cell buses has been made over the past five years, this technology is still more expensive, less durable and less reliable than conventional internal combustion (diesel) engine technology. For PEM fuel cell buses to become the preferred option for transit agencies, improvements in fuel cell durability, system reliability, and reduced cost are essential. Once these are achieved, the market for larger fuel cell bus fleets will grow and this technology will begin to replace the incumbent, but more polluting and less efficient, internal combustion engine technologies. While membrane durability is the primary life-limiting component in

PEM fuel cell bus operation, improvements are also needed in other components of the system.

Ballard discovered that the H2 sensors in the HD6 fuel cell module had much shorter lifetimes than initially predicted. This sensor is a component of the fuel cell safety system used to ensure that hydrogen leaking from the anode to the cathode of a PEM is detected. This is particularly important to prevent flammable or explosive concentrations of hydrogen from being exhausted to the environment. These initial modules had been sitting idle for several months before installation, during which time the sensors had noticeably degraded. Calibration of the sensors on buses in use, on their regular maintenance schedule showed the sensors were becoming less sensitive, some failing after only 600 hours of operation, although the variation in lifetimes was large, with some sensors lasting over 2000 hours. This result was unexpected since the identical sensor degraded very slightly in Ballard's previous design of the fuel cell module (P5). The degradation rate in the new modules was unacceptable.

1.1.1. Objectives

The research presented in this thesis focuses on developing reliable and low cost diagnostic systems that meet the safety requirements of heavy duty fuel cell systems, specifically by lengthening the useful life of the cathode exhaust hydrogen concentration sensor. The purpose of lengthening the life of this sensor is to increase its reliability, reduce component cost over the bus lifetime, and reduce the required frequency of manual sensor calibrations in the maintenance shop.

The methods of protecting the hydrogen sensor strongly resemble the Workplace Hazardous Materials Information System (WHMIS) suggested methods of human protection from hazardous materials – removal, distance, protection, and treatment. The best method suggested is to remove the hazardous material, the siloxanes from the silicone hoses. This can be done by either changing the piping material or baking out the silicone hoses to medical grade. Both these methods were looked at by Ballard and rejected due to the positive properties of the current hoses and the cost of baking the siloxanes from the hoses. The second method suggested by WHMIS is to move the subject (the hydrogen sensor) away from the hazardous materials. Ballard did attempt

this by removing the sensor from the main cathode exhaust and placing it in a small bleed line parallel to the exhaust to reduce the amount of siloxanes that have access to the sensor. The gas stream in this line still has the same makeup as the gas in the cathode exhaust, meaning the siloxane contaminates are still present. This change did reduce the degradation rate of the sensor by reducing the volume of siloxanes present. Since it was still exposed to siloxane there was still degradation and, thus, additional gains were sought. The third method suggested when the other two are not feasible is to wear Personal Protective Equipment (PPE). This protection method is implemented by installing an activated carbon filter on the sensor to protect it from the siloxanes, thus acting as PPE.

Sometimes all of these precautions fail, and the subject suffers harm from the hazardous material. In this situation, a good healthcare system allows for treatment of the harm. This corresponds to the last method examined in this thesis – recalibrating the sensor as it degrades.

1.1.2. Thesis Outline

The thesis is divided into five chapters. This first is introductory and background material, describing how fuel cells work in general, introducing some key components of Ballard's current fuel cell module and safety systems, particularly the cathode exhaust hydrogen concentration sensor. Chapter 2 examines how a physical filter can reduce sensor degradation by scrubbing the poisons that degrade the sensor from the gas flow, how long the filters can last, and signal reduction due to fuel suppression of the filter. This method has significant value, and is already being trialed in the current bus version for the vent sensor. A method to calibrate the sensor by comparing the sensor output with calculated concentrations of hydrogen is discussed in chapter 3. A proof-of-concept test was performed and shows that under certain conditions, the sensitivity of the sensor could be measured in-situ. Chapter 4 gives the conclusions and discusses future work required to see this knowledge implemented in industry. A final chapter is included to changes are anticipated in future bus modules or would need to be changed in order for the in-situ calibration method to be accomplished completely.

Note that Appendix A discusses another attempted method to calibrate the sensor using intelligence directly on the real time sensor signals to detect either true hydrogen concentration from degraded sensors or to determine the level of degradation of the sensor. The various ways attempted and some possible reasons this method did not work, such as dissimilarities in sensor degradation from bus to bus, are discussed.

1.1.3. *Basic Fuel Cell Operation*

Fuel cells are galvanic cells that operate with reactants flowing across the electrodes, as illustrated in Figure 1. One of the most ubiquitous types of fuel cells is the low temperature PEM fuel cell because of its wide range of potential applications. This is due to its low operating temperature, high efficiency, and fast startup. This is the type of fuel cell that Ballard focuses on.

The core of the Ballard® fuel cell, as shown in Figure 1, consists of a Membrane Electrode Assembly (MEA) placed between two flow field plates (labelled A and H). The MEA consists of two electrodes, the anode (C) and the cathode (F). Each side of the membrane (E) is coated with a thin catalyst layer and a gas diffusion layer. The flow field plates direct hydrogen to the anode and air to the cathode. When hydrogen reaches the catalyst layer, it separates into protons (hydrogen ions) and electrons (Equation (1)). The free electrons, produced at the anode, are conducted as a usable electric current through an external circuit. At the cathode, oxygen from the air, electrons from the external circuit, and protons transferred across the membrane combine to form water and heat (Equation (2)). The water formed continues out of the cathode side of the fuel cell to the environment.
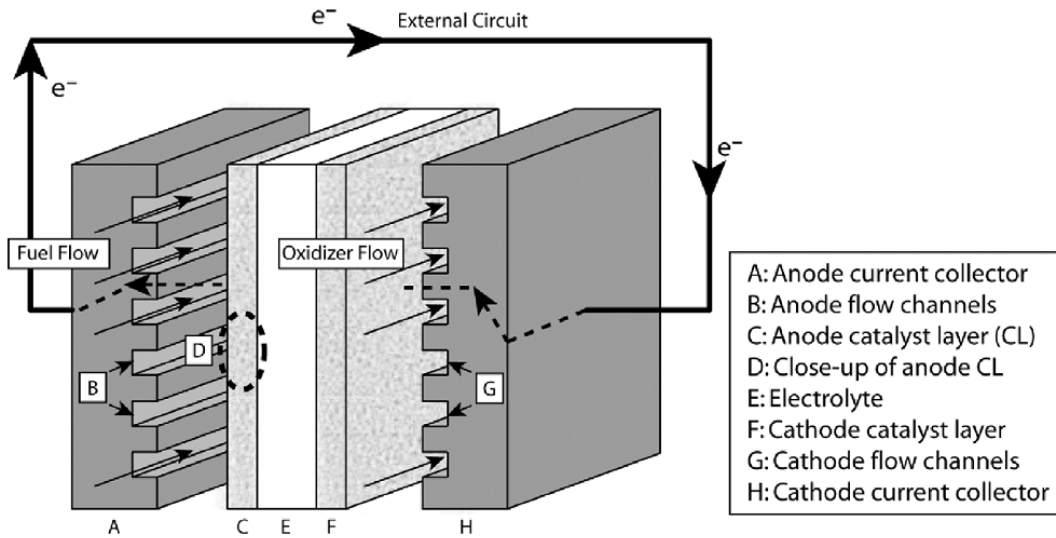
Figure 1 Basic parts of a fuel cell [1]

$$H_2 \rightarrow 2H^+ + 2e^-$$ (1)

$$2H^+ + \frac{1}{2}O_2 + 2e^- \rightarrow H_2O$$ (2)
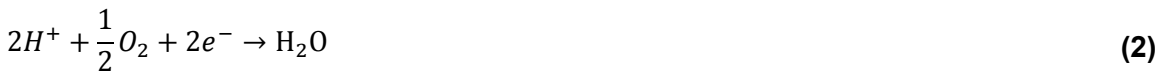
1.1.4. Fuel Cell Operation Specific to Ballard Buses

Ballard's HD6 fuel cell module is a sealed box containing one or two Mk1100 fuel cell stacks, which consist of layers of cells in series. The module also includes the related processes listed in Table 1. A schematic of the Process and Instrumentation Diagram (P&ID) for the Ballard HD6 PEM fuel cell module is shown in Figure 2, where the different colours in this figure are different circuits as defined in Table 1.

Table 1 Circuit identification of PEM P&ID

Process	Colour
Process air circuit	Green
Hydrogen circuit	Red
Spray water (humidification and product water recovery) system	Blue
De-ionized glycol (cooling) system	Black
Controls	Aqua
DC power circuit in	Magenta
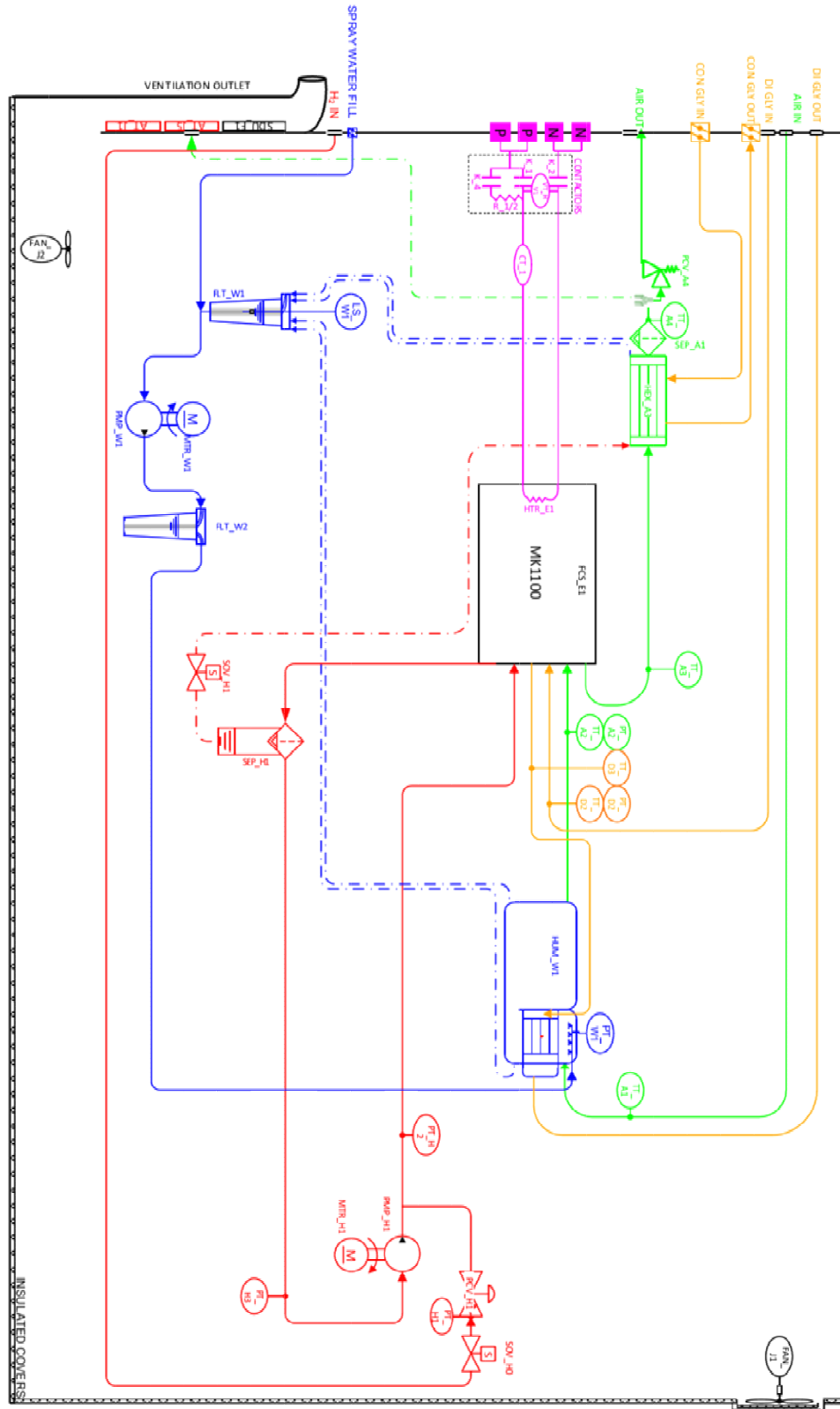
Figure 2 Simplified Process & Instrumentation Diagram of the Ballard HD6 module

The flows into the module include air to the AIR IN port, hydrogen to the H2 IN port, and coolant to the DI GLY IN (main cooling) and CON GLY IN (condenser cooling) circuits. Fuel is fed to the stack through a bias regulator (PCV_H1) that maintains a small fuel pressure bias to the anode above the air pressure supplied by the compressor to the cathode. Fuel utilization is enhanced with a hydrogen recirculation blower (PMP_H1) that circulates the hydrogen through the anode loop as it is being utilized by the stack. This maintains a near uniform high concentration of hydrogen throughout the anode.

In operation, as the fuel is recirculated in the anode loop, small amounts of nitrogen and water diffuse across the membrane from the cathode (air) side of the cells against the pressure gradient into the anode. These builds up in the anode loop to a concentration of about 20% nitrogen and some liquid water. This reduces the hydrogen partial pressure, necessitating the purging of some of this gas from the anode through the water separator SEP_H1 and the solenoid operated purge valve SOV_H1 to bring the anode hydrogen concentration back up to an optimum level. The purged gas and water mixture is injected into the cathode exhaust flow coming from the PEM.

The MEAs in the MK1100 stacks, shown in Figure 2, use commercially available perfluorosulfonic acid (PFSA) membranes. This membrane can also deteriorate, allowing hydrogen to leak into the cathode. Most of these leaks are very small and do not affect bus performance or hydrogen utilization rate. However, due to the potential for larger hydrogen leaks from a degrading membrane, the safety system includes the hydrogen concentration sensors. The cathode exhaust hydrogen sensor discussed in this report is AT_J5 in the diagram. This sensor is in a sample line which bleeds off a small quantity of cathode exhaust gasses upstream of the cathode back pressure valves (SOV_A4, PCV_A4). This sensor, along with the module ventilation hydrogen sensor (AT_J1) is located inside an access panel on the module. Should a fire occur in the module, it would be detected by the ventilation fire alarm (SDU_F1), located on the same panel.

1.2. Fuel Cell Safety Systems

As the power plant in an automotive application, the HD6 fuel cell module must meet required safety criteria. The safety systems are especially relevant since the fuel, hydrogen, requires very little energy to ignite and is flammable at concentrations as low as 4% and up to 75% [2] in air. In addition, it is the smallest element and is in gaseous form, so it is very difficult to contain. It is important to avoid the buildup of hydrogen in any enclosed area and to prevent hydrogen concentrations from reaching flammable levels. In this section, the various safety issues and mitigation mechanisms are discussed.

1.2.1. Safety Issues

1.2.1.1. Short circuits heat and burn

Short circuits result in very high current flow in the fuel cells. The heat generated can start a fire, either of hydrogen or of other flammable materials. The fire alarm is used for this.

1.2.1.2. High voltage / high current alarm

When the fuel cell is in a high voltage or a high current state the PEM membrates degrade more rapidly. The current and voltage are monitored, and when the fuel cell is in an unacceptable range, alarms on the current and voltage sensors are triggered.

1.2.1.3. Internal Hydrogen Leaks

The membrane (E in Figure 1) is designed to allow ions (hydrogen protons) to diffuse across it, but to be an insulator for electrons and molecules. One of the major modes of failure of fuel cells is the deterioration of the MEA. The anode is kept at a slightly higher pressure than the cathode so that if there is a leak, hydrogen will cross to the cathode instead of air to the anode. Hydrogen in the cathode has minimal lasting repercussions since it oxidizes rapidly, while air crossing to the anode can cause cell reversals which result in sudden, catastrophic failure of the membranes.

1.2.1.3.1. Small Leaks

As noted, deterioration of the fuel cell PEM membranes during use causes small internal fuel cell leaks. Losses of minor amounts of hydrogen fuel are not significant for fuel efficiency of the fuel cell, but larger leaks present a safety hazard. Small holes in the membrane allow only small amounts of hydrogen to cross to the cathode, and even with larger holes near the leading edge of the membrane, all the hydrogen that crosses over the cathode side recombines with the air on the MEA catalyst on the cathode side. These holes reduce the efficiency, but are not a safety risk to the system, and are not detected by the hydrogen sensor, as the hydrogen has been oxidized.

However, because hydrogen leakage in a PEM fuel cell stack is unavoidable, there is always an accepted leak rate to work with [3]. When the leak exceeds the safe threshold, the hydrogen concentration in the cathode approaches the flammability limit and the hydrogen sensor triggers an alarm which shuts down the fuel cell module.

1.2.1.3.2. Reversals/Catastrophic Leaks/Shorts

Fuel starvation presents a more serious condition. Fuel starvation is an insufficient supply of hydrogen into the anode, which, in PEM fuel cells is usually associated with a drop in voltage and cell potential reversal. Fuel starvation is one of the most damaging sources of cell reversal of the membrane-electrode assemblies (MEA). Such a cell reversal will produce oxygen instead of oxidizing hydrogen in the anode which, in turn, causes local heat generation of the membrane. This heat generation causes a burning reaction resulting in many pin-holes along with larger holes in the membrane. With the hydrogen pressure higher than the air pressure, there is a very high leak rate of hydrogen to the cathode side, which can cause the hydrogen concentration to exceed the flammability threshold.

1.2.1.4. External Hydrogen Leaks

Hydrogen can also leak out of the fuel cell into the surroundings. The seals on the hydrogen recirculation blower are the most common problem, but leaks can occur at any joint/seal. Electrical short circuits have caused such intense overheating that the graphene fuel cell plates have burned through, resulting in a massive external leak. The fuel cell stack is enclosed in the HD6 module container. Fans (FAN_J1 and FAN_J2) in

the module ensure that the module itself remains below hydrogen's flammability limit, and the module integration manual explains that the module must be used in a ventilated area [4].

1.2.2. *Internal Hydrogen Leak Detection*

Several different types of leak detection methods have been utilized. The large number of cells makes it difficult to localize the leak unless there is leak detection on each individual cell. The cost and complexity of individual cell leak detection is prohibitive, which leads to leak detection of the entire stack, where one small leak in one individual cell is difficult to detect due to many other factors affecting sensor readings. Several of the leak detection methods are discussed below.

1.2.2.1. Cell Voltage Monitoring

Cell voltage monitoring (CVM) is a method of monitoring the health of each cell in a fuel cell stack. If one cell's voltage starts dropping, it indicates catalyst degradation, hole formation (H_2 crossover -> low O_2 concentration), or fuel or air flow blockage. While this method is invaluable as a service shop based diagnostic procedure, and works for stationary systems, it is not robust enough for the HD application and is not used.

1.2.2.2. Electrochemical Impedance Spectroscopy

Electrochemical Impedance Spectroscopy is a system used widely as a research tool for membrane development [5]. This method applies an alternating current or voltage across a single cell. The measured voltage or current is used to characterize the membrane conditions. The output of this method gets smeared when multiple cells are used in a stack, and the problem is thus less evident. Prototypes of this method are in use and further research is ongoing [6,7].

1.2.2.3. Voltage Bleed Down

A rough estimate of leak rate can be achieved by comparing the time it takes for the voltage of a fuel cell to "bleed down" after turning the fuel cell off. The speed of the voltage drop indicates the size of the leak [8].

1.2.2.4. Hydrogen Concentration Sensors

The most common method for detecting hydrogen leaks are hydrogen concentration sensors. The hydrogen concentration sensors need to be accurate to reliably detect when the cathode approaches the flammability threshold. Unfortunately, hydrogen sensors are expensive and degrade over long periods of time. However, because it directly measures how closely the hydrogen concentration is to the flammability limit, and the hydrogen concentration is the direct result of hydrogen leaks, it is a preferred method for leak detection.

Boon-Brett et al in [9] provide a comparison of various hydrogen sensor types for automotive and stationary applications, and outline the gaps between current sensor technologies and industry requirements. They showed that the detection limit, accuracy, and environmental stability of current sensor technologies meet the automotive industry requirements. However, the 15 year lifetime requirement cannot be met by any of the examined hydrogen sensors. In [10], Boon-Brett et al analyzed the reliability of various hydrogen sensor technologies and suggested that the maturity and good performance of hydrogen sensors makes them a suitable candidate for automotive applications.

To improve the lifetime of hydrogen sensors, Mor et al in [11] proposed using UV light to clean a titania-nanotube hydrogen sensor when it is contaminated with motor oil and/or stearic acid. In [12], Hughs et al used a physical model of the sensor along with thermal measurements to calibrate a palladium-nickel film resistive hydrogen sensor and showed accurate results.

Different types of sensors experience varying amounts of degradation and drift with time and environmental effects, reducing the accuracy of measurements. Manual recalibration is time-consuming and expensive, so redundant measurements are often used as a method to check the consistency of signals [13,14]. This works especially well where the sensor of interest can be calibrated using a calibrated mobile reference sensor. For some situations, re-calibration in-situ is ideal. This can be done automatically when calibration gas is available [15], and the sensor can be tested against clean air and a calibrated gas. Neural networks and fuzzy logic have been used to incorporate artificial intelligence to gas sensor calibration. These techniques have

been used as standalone calibration techniques [16], and used for state prediction in conjunction with redundancy to statistically validate measurements [17].

Several types of hydrogen sensors are available. Ballard Power has selected the Riken Kieki Instruments (RKI) FSD 753 unheated hydrogen sensors and FHD 752 heated hydrogen sensors for implementation in their fuel cells. The fuel cell module in Figure 2 shows the two hydrogen concentration sensors. The AT_J1 is an unheated sensor located at the outlet vent of the module and is used to detect external leaks. The AT_J5 is a heated sensor in the cathode exhaust used to detect internal leaks.

The hydrogen sensors give a warning if the cathode exhaust has 2% hydrogen concentration for 5 seconds and is set to alarm if the concentration remains above 3% for 10 seconds. The temporal setting prevents the cathode exhaust from triggering an alarm on start-up when hydrogen, which crossed over to the cathode while the module was shutdown, gets exhausted from the cathode.

Due to the high cost of the RKI sensors, other, less expensive sensors have been examined. The characteristics of the RKI sensors and a sensor manufactured by NTM are outlined below.

1.2.2.4.1. RKI Specifications and Characteristics

Both Riken Keiki FSD753 and FHD 752 sensors have a resistive catalytic bead connected as one element of a Wheatstone bridge. These sensors detect 0-4% H2 by volume with a linear output signal of 0.5-4.5V. The specification sheet for a new sensor is shown in Appendix C. If the sensors are not recalibrated during their lifetime, the signal decreases as the sensing bead gets covered with silica, and the sensor can give false negative readings.

1.2.2.4.2. NTM Specifications and Characteristics

The NTM SenseH$_2$ sensors have a chemi-resistive ceramic sensing element. They are less expensive, but have a shorter life. The sensor signal increases with time for the same hydrogen concentration, so there is a potential for false positives if it is not calibrated frequently enough. These sensors detect 0.25-4% hydrogen in air, corresponding to 1.0-4.5V. The voltage output increases in half volt steps corresponding

to an increase of approximately $^2/_3$% hydrogen. The technical specifications of the NTM sensors are shown in Appendix D.

1.2.2.4.3. Ex-situ Calibration Methods for Hydrogen Sensors

In order to quantify the effect of filtering and auto-calibration on the hydrogen sensors under test, a test station was used to measure the accuracy of the hydrogen sensors. For this purpose, the sensors were exposed to hydrogen mixtures from Praxair cylinders with concentrations of 1% +/- 0.01%, 2% +/- 0.02%, and 3% +/- 0.03% hydrogen. The exposure time was a 30-second cycle at each concentration repeated 3 times. The average signal at the steady state values were used to obtain the calibration of the sensors. An example of a hydrogen sensor calibration is shown in Figure 3. The curves for these sensors are almost linear except when very degraded, and, hence, a single linear calibration value was used to characterize the sensitivity of each sensor.
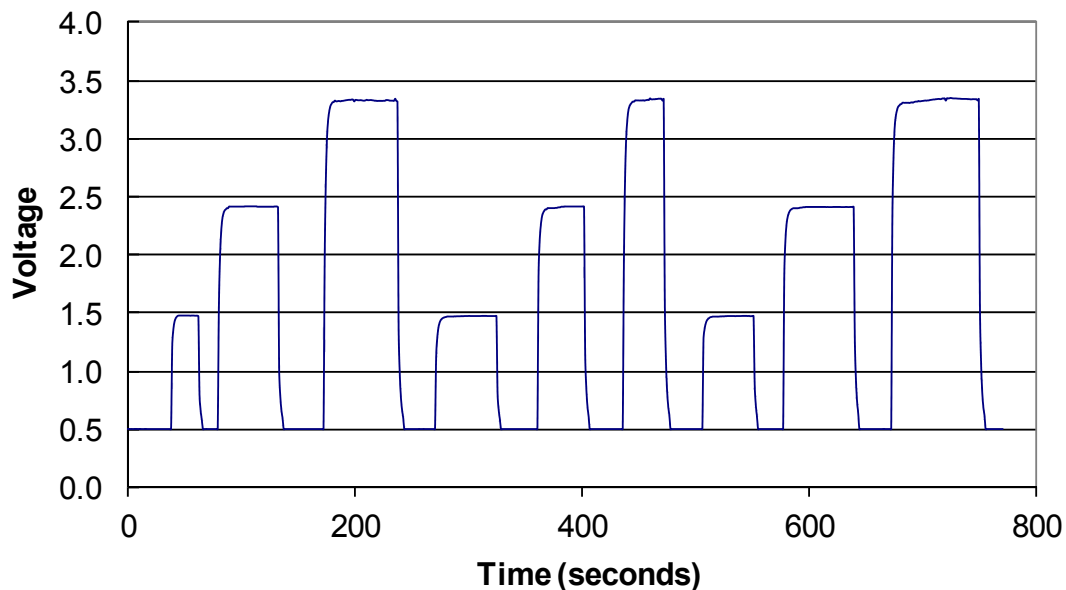
Figure 3 Example voltage measurement for calibration of RKI hydrogen sensor

Sensors are considered degraded and no longer useful when the output signal is degraded to 20% of the original value. The degradation is determined by exposing the sensor to 2% hydrogen during regularly scheduled maintenance checks. This level of degradation is chosen because the currently implemented vent and exhaust alarms are

at 50-75% Lower Flammability Limit (LFL) respectively, and at 20% degradation, the hydrogen concentration would actually be 62-94% LFL when the sensor alarms. If the sensor degraded any further, the cathode exhaust sensor would not alarm even when there was a flammable mixture in the cathode exhaust. In-situ calibration can lengthen the useful lifetime of the sensor while reducing time consuming manual calibration.

1.2.3.   Sensor Degradation

The first HD6 fuel cell modules had sat idle for several months before installation. Calibration of the sensors after installation on their regular maintenance schedule showed the sensors were decaying. The variation in lifetimes was large, with some failing after only 600 hours of operation, while other lasted upwards of 2000 hours. On the previous iteration of the fuel cell module for buses (P5), the hydrogen sensors degraded perceptibly, yet slowly enough to allow acceptable length of operation and appropriate warning and alarm triggers. It was known that siloxanes were the cause of the degradation in the P5 busses, so siloxanes were the first suspect investigated in the failure analyses of these hydrogen sensors. The HD6 module had large silicon hoses that were not present in the P5 bus, so these were investigated.

Failure Analysis on a failed sensor from one of the bus modules showed an accumulation of contaminants on a polytetrafluoroethylene (EPTFE) membrane separating the sensing element from the environment. A scanning electron microscope (SEM) image of the surface of the membrane showed that, though graphite filaments from the Membrane Electrode Assembly (MEA) were present on the surface along with other residue, the pores in the EPTFE were for the most part accessible. To determine the composition of the residue left on the EPTFE cover, an Energy Dispersive x-ray Spectroscopy (EDS) was performed on two sections of the cover, one area with residue, and one clean area. The EDS showed the main contaminants were oxygen and silicon. Much smaller trace signals indicated slight steel, brass, and aluminum contamination. However, since the pores through the EPTFE membrane are mostly clear showing that the level of residue on the cover is not attenuating the signal, examination turned to the sensing bead.

While signs of degradation were not apparent on the palladium sensing bead of the hydrogen sensor to the naked eye, the SEM images showed that siloxanes had adsorbed on the surface of the palladium bead. An EDS examination showed raised levels of silicon as compared to a new palladium bead. Positive ion mode Time-of-Flight Secondary Ion Mass Spectrometry (TOF-SIMS) shows that most of the ion signal is attributable to silica (SiO2) on the surface of the bead. The siloxanes had oxidized to silica on the bead. Hexamethylcyclotrisiloxane (HMDSO), one of the siloxanes found in later testing, oxidizes to silica according to Equation (3).

$$((CH_3)_2SiO)_3 + 12O_2 \rightarrow 3SiO_2 + 6CO_2 + 9H_2O \tag{3}$$
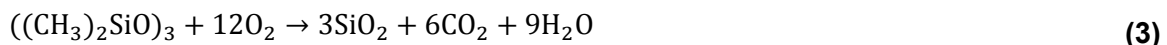
The silica prevents hydrogen from reaching the bead underneath the silica thereby reducing the output signal. Since this is a surface contaminant, the makeup and resistance of the bead do not change.

Some of the components (seals and silicone tubes) in the HD6 fuel cell module but not in the P5 module were considered likely to off-gas the siloxanes which result in the silica buildup on the hydrogen concentration sensors. A preliminary test was then performed on a few different materials used in the module. These included a silicone hose, double sided tape and foam. These items were enclosed in a sealed bag with two new sensors. These sensors showed rapid degradation of the sensor signal, indicating that these items were indeed the source of the degradation, though the degradation was inconsistent from sensor to sensor.

It is well known that Activated Carbon can remove volatile organic compounds and siloxanes. Ballard created an activated carbon filter made from a FRAM Automotive Cabin Air Filter (PN CF8813A). The effectiveness of activated carbon as a protective layer over the sensor was examined by adding several layers of activated carbon to the sensors. This filter is discussed in the next chapter and shown in Figure 4.

This preliminary testing confirmed the adverse effect of siloxane off-gassing on the hydrogen concentration sensors, causing the output signals of the hydrogen sensors to decrease for a constant hydrogen concentration. As siloxane particles are released into the air, and more so during start-up and shutdown operations of the bus due to temperature changes in the hose, the effect is greater on the cathode exhaust sensor

15

and, thus, becomes the sensor of interest in this research. The focus of further testing for sensor failure is directed towards understanding and minimizing the impact of siloxane degradation on the hydrogen sensors and on the integrity of sensor signal reading.

2.   Sampled Gas Filtration

Following the WHMIS example of Section 1.1.1, this section describes a method for isolating the sensor from its environmental hazards. Preventing siloxanes from reaching the sensor head using a filter would prevent sensor degradation. The method of choice is to use filters to collect the off-gassed siloxanes, purifying the sample gas stream prior to the gas reaching the sensor. Eventually, as the active filter area is used, the filter becomes saturated and needs to be replaced or, once again, the sensor will begin to degrade.

To determine the effectiveness of the filters in protecting the sensors, accelerated testing was performed. Filtered and unfiltered sensors were subjected to siloxane contaminated atmosphere, and the sensor calibration monitored. This measured the level of protection and the duration of protection.

2.1. Filtration of Siloxanes

The filters tested here both use activated carbon as the active component for removing siloxane particles. This section discusses what filters were used, and how they were tested.

2.1.1.   Ballard Filter

The "Ballard filter" is essentially a circle of activated carbon (FRAM Automotive Cabin Air Filter, PN CF8813A) fit over the top of the sensor. A steel washer is used to hold it down, and a piece of Tygon tubing is friction fit around the sensor and the washer to hold the filter in place, as seen in Figure 4. It was used for the initial tests, and, when it was shown to work, RKI provided a filter of their own.
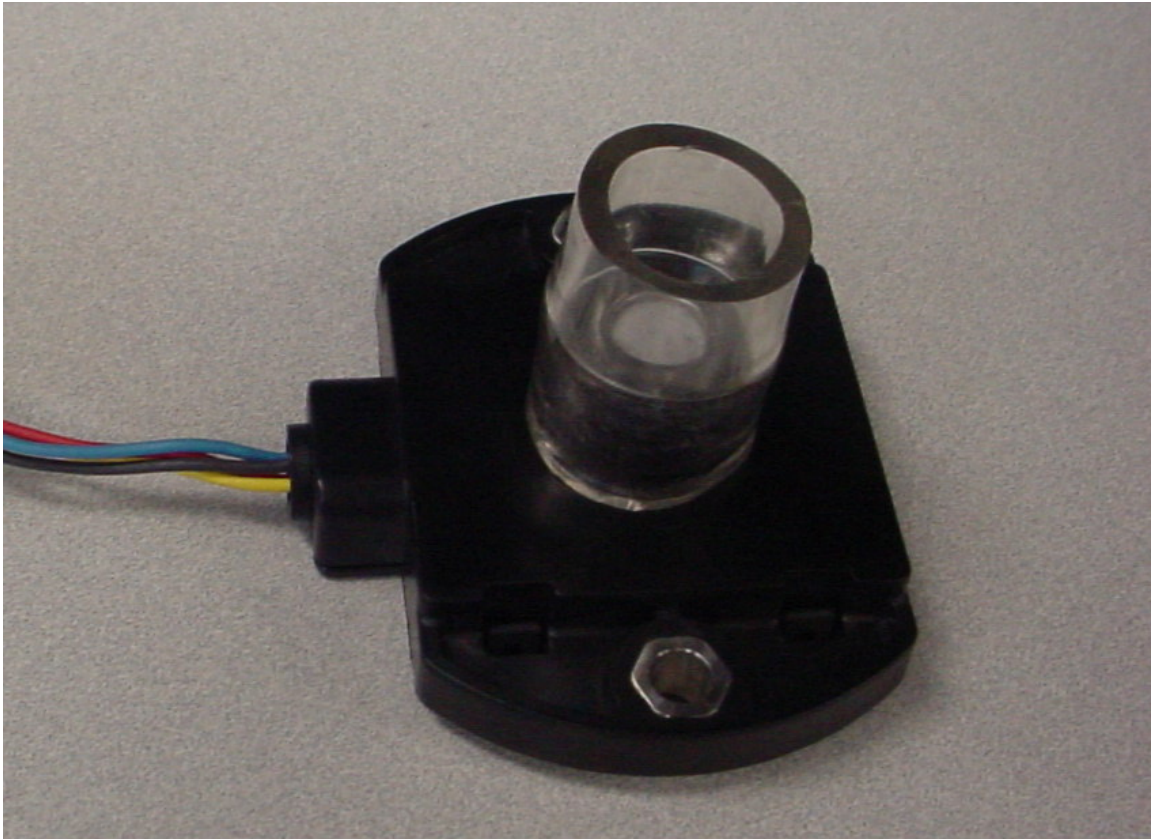
Figure 4 Sensor with Ballard filter

2.1.2.   RKI Filter

Once the Ballard filter verified the improved sensor life, the results were shared with RKI, their supplier of hydrogen sensors. Based on these results, RKI developed a filter that integrates well with the RKI sensor. The RKI filter also uses activated carbon, but is covered by an EPTFE cover to keep liquid water out. A moulded rubber cap holds it in place over the sensor. Installation of the sensor is described in Appendix E.

Figure 5 Sensor with RKI filter

2.2. Test Procedure

As it takes many hours of operation for a hydrogen sensor to degrade under normal operating conditions, an Accelerated Stress Test (AST) was designed to increase the rate of sensor degradation, examine the effectiveness of various filters and understand the factors affecting the rate of siloxane released into the air from the silicone hoses. Since most of the siloxane release occurs during temperature cycling of the hose, such as at bus start-up and shutdown, the accelerated test used frequent temperature cycling.

The test apparatus consisted of a silicone hose enclosed in a Plexiglas box with a steel sensor manifold bolted to the top. The sensor manifold was designed to hold 5 hydrogen sensors simultaneously. This setup is shown in schematically in Figure 6.
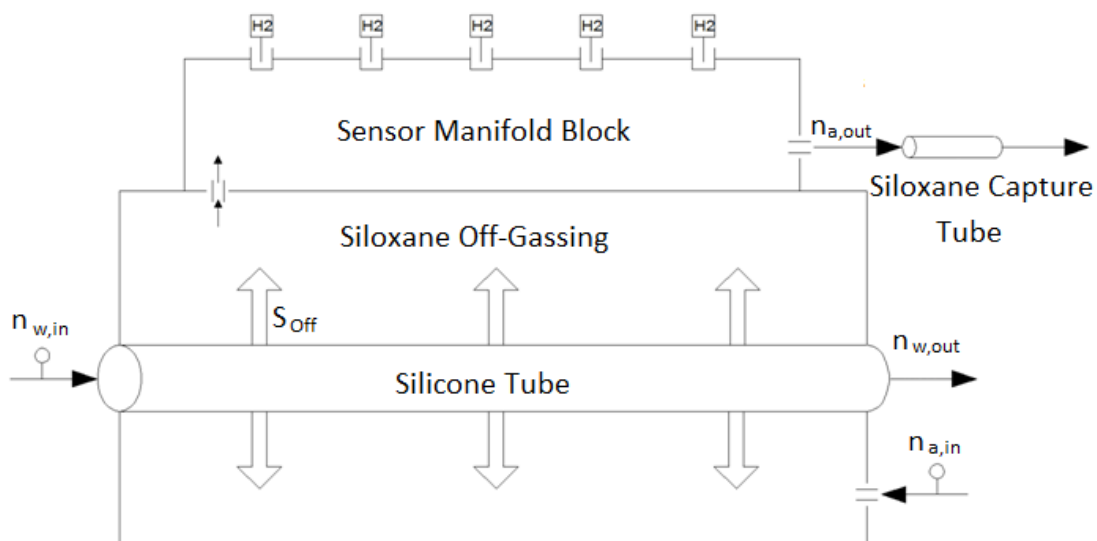
Figure 6 Experimental setup for siloxane filtering testing

As initially configured, air ($n_{a,in}$) enters the box at a rate of 0.250 SLPM and the siloxanes off-gassed from the outside of the hose are picked up by the air. The air then travels into the sensor manifold block past the hydrogen sensors. Finally the air exits the outlet port where it is directed through the SKC Anasorb Carbon Sampling Tube used to filter the siloxane from the air. Lastly, the air is bubbled through water as a visual observation of continuous flow and a check that there are no leaks in the test setup. The temperature cycles and flow rate are shown in Figure 7. The siloxane chemical composition and concentration in the air sample was determined by sending the Anasorb Carbon sampling tubes to an external lab for accurate assessment (Section 2.2.1 Siloxane Release Rate).
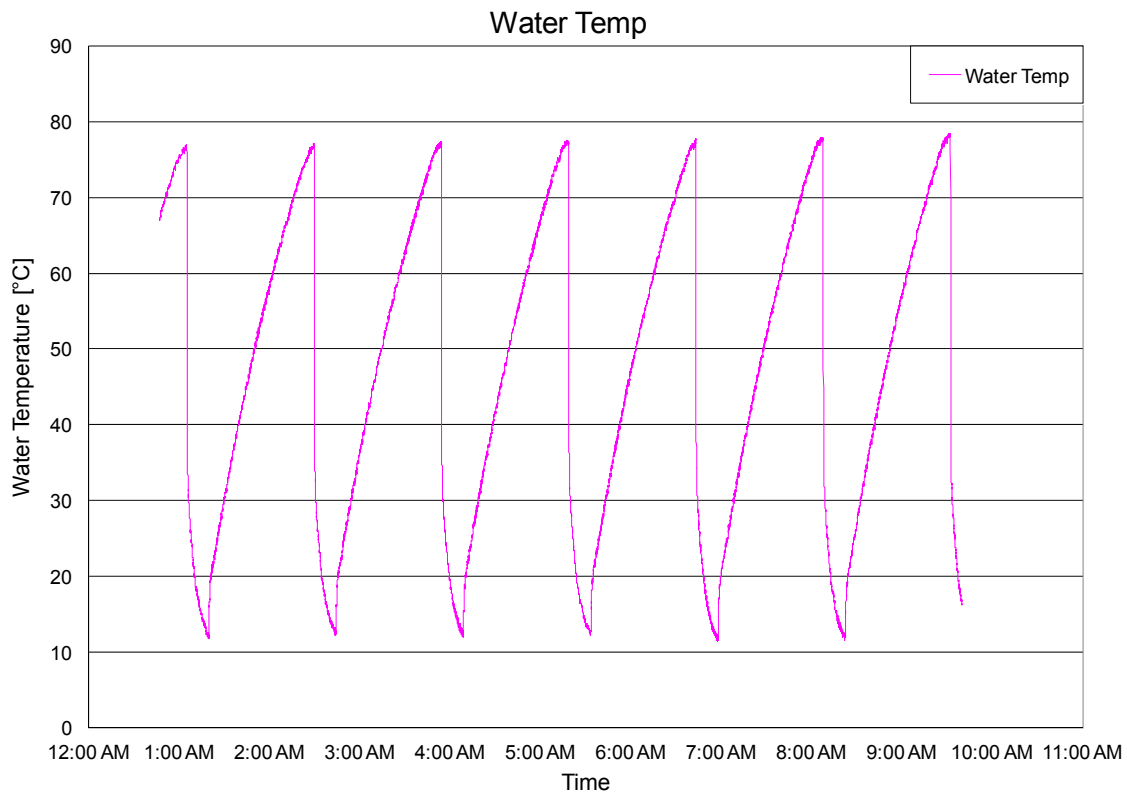
Figure 7 Accelerated Stress Test Heating & Cooling Cycles

As the test progressed, the air flow was reduced to 0.050 SLPM to further increase the siloxane concentration in the air and further speed the degradation of the hydrogen sensors.

Figure 8 is a photograph of the test setup shown schematically in Figure 6. The five sensors examined in this test are 4 RKI Model FSD-753 Hydrogen Sensors and one heated RKI FHD-752 sensor, each of which can detect hydrogen concentration in the range of 0-4% by volume. These sensors are in the black manifold box at the top of Figure 8, above the Plexiglas box enclosing the green silicone tube. Two of the sensors have activated carbon filters supplied by RKI, one sensor has a filter manufactured by Ballard, and two sensors are without filters as control samples (one of which is the heated sensor). The degradation rate of the unfiltered sensors in the test were compared to the average sensor degradation rate on operating busses to estimate the increased rate of degradation of this test. The test was also used to provide guidance for how long the RKI-supplied filters should last in field conditions.

21
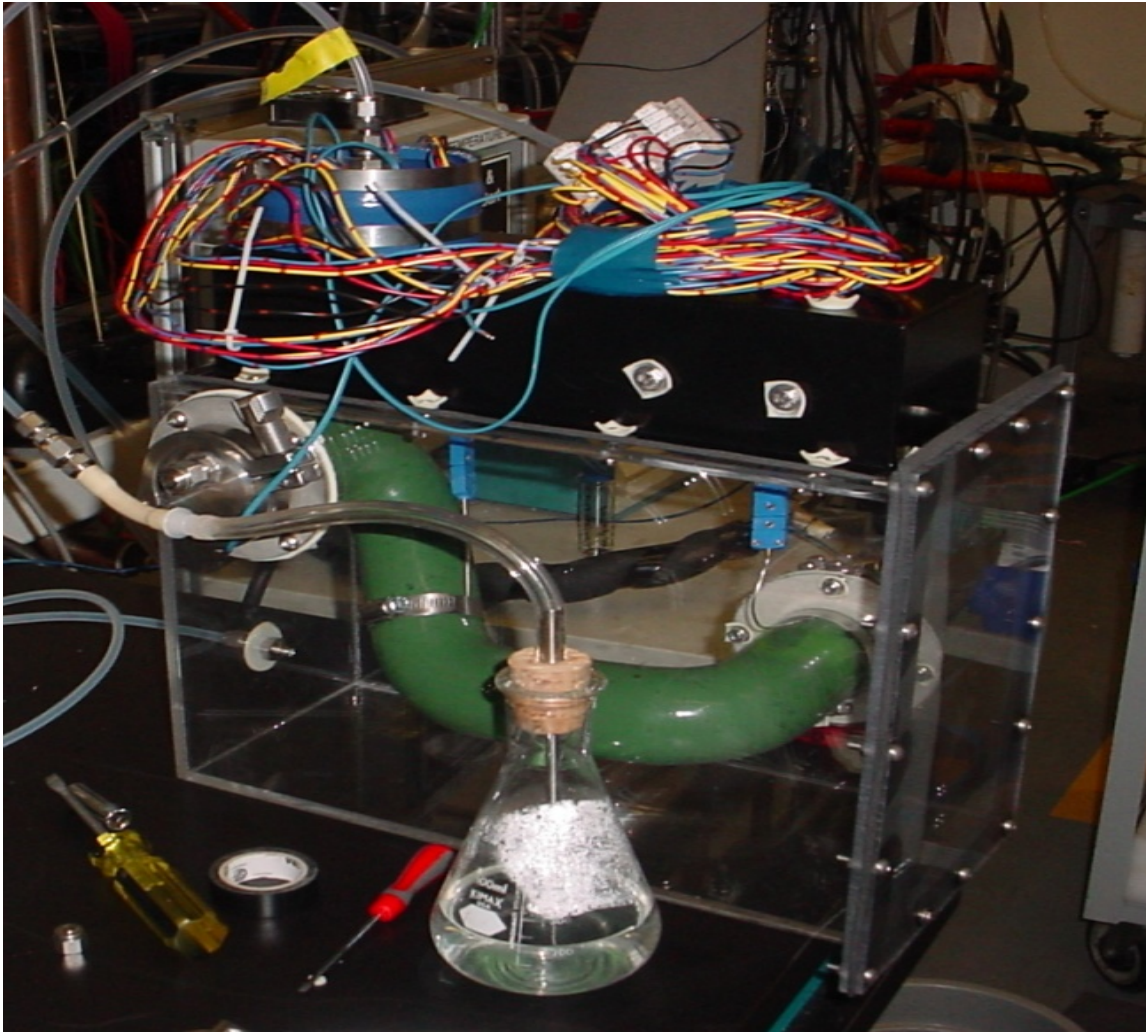
Figure 8 Siloxane release test setup

The test continued until the majority of the sensors reached the "failed" state of 20% degradation, which gives a reading of 1.6% hydrogen when the actual hydrogen concentration is 2%. It took about 4 months of continuous testing before all the sensors degraded and thus complete the test.

2.2.1.   Siloxane Release Rate

The test progressed through discrete time periods. For the first two time periods, the air flow rate was 0.250 SLPM. The remainder of the time the air flow rate was reduced to 0.050 SLPM. All of the air exhausted from the test apparatus went through the Anasorb Carbon filter, where all of the siloxane was removed. The airborne

concentration of siloxanes found from the mass divided by the flow rate is plotted in Figure 9. The types of siloxane were also determined, and are available from Ballard if required. Figure 9 shows that the siloxane concentration went up when the flow rate was reduced. However the concentration then stabilized back at approximately 9-10 µg/L, if we ignore the low concentration outliers.
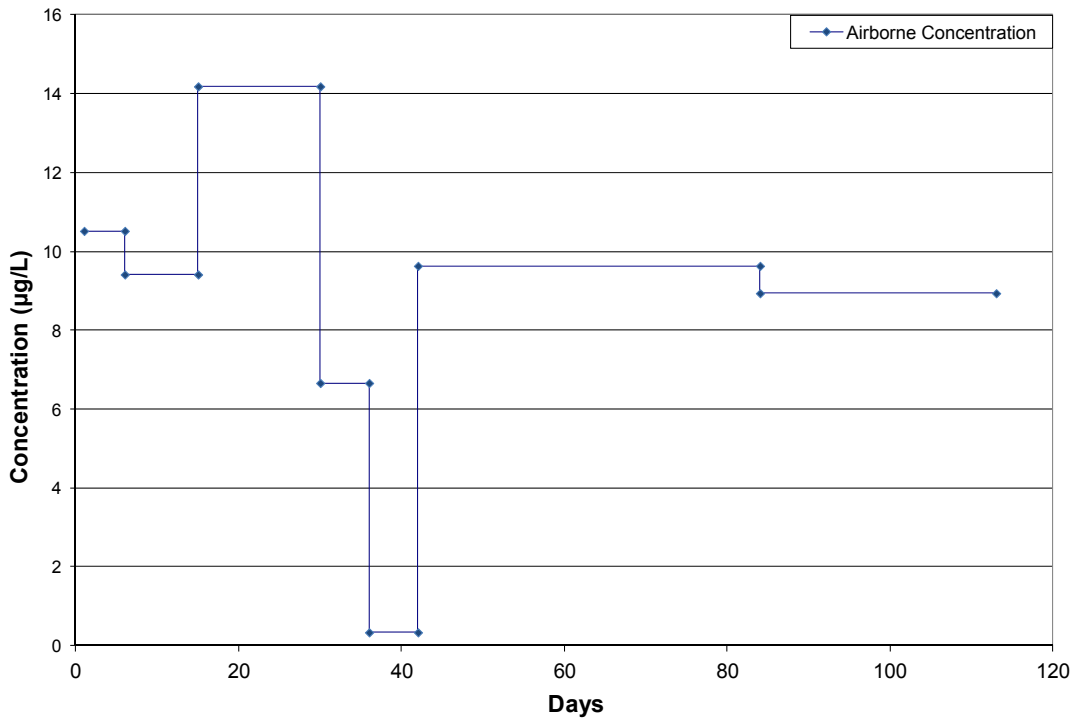
Figure 9 Airborne siloxane concentration during the test

Every 15-20 days of temperature cycling a full day of measurements was performed to determine a more instantaneous siloxane release rate. Once the siloxane release rate testing was done, a new tube was installed for the next period of testing. The sensors were also calibrated each time the collection tube was replaced by substituting the air with 0.25 SLPM of 2% +/- 0.01% hydrogen from a Praxair cylinder of compressed gas.

The siloxane release rate is expected to be a function of the temperature and to decrease as a negative exponential as the siloxanes leave the hose. The internal siloxanes would then diffuse through the hose to the exterior. If the third, sixth, and

seventh segments are viewed, the negative exponential effect can be seen. For this to be the case, the fourth and fifth segments must be considered outliers.

2.3. Results

Figure 10 presents a graph of the observed sensor degradation over the course of the entire test. These test results are from the sensor output signals, when the sensors were calibrated with 2% hydrogen. When signals are averaged, the curve error bars show the average and range of the signals. The curve with the highest initial signal voltage is that of the unfiltered control sensors. This shows that the activated carbon filters initially reduce the signal by reacting with some of the hydrogen thus reducing the hydrogen concentration at the sensing element.
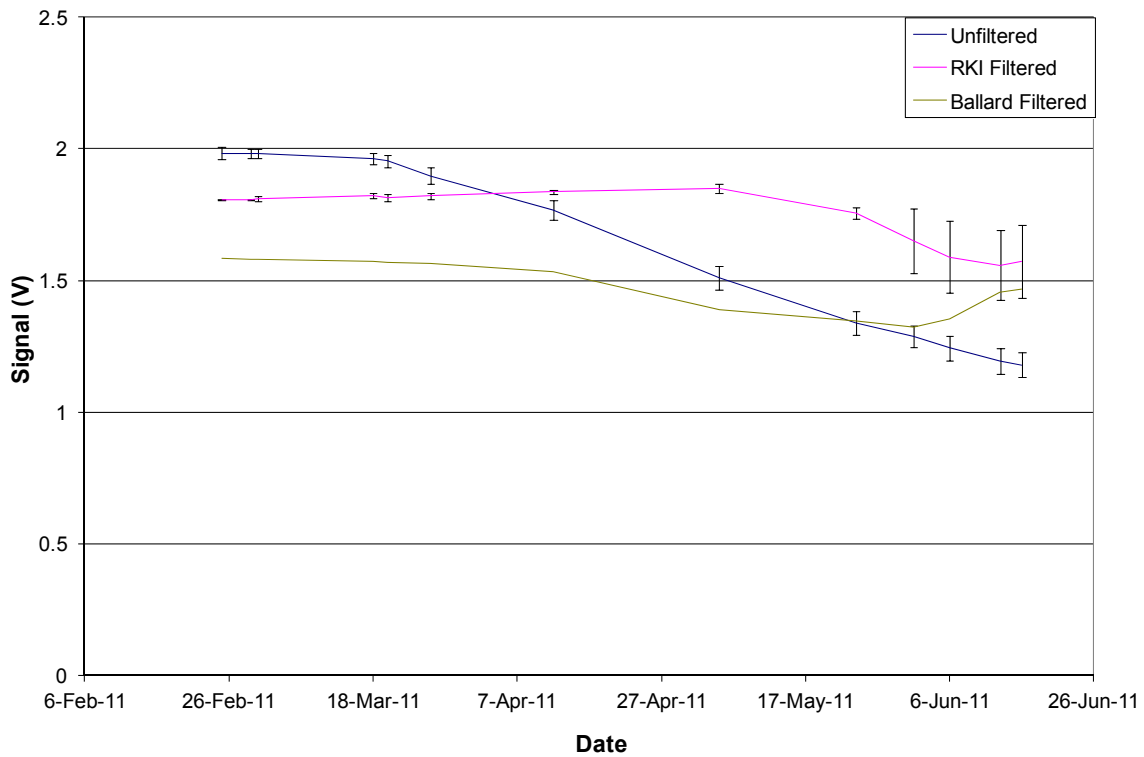
Figure 10 Effectiveness of filters on hydrogen sensor lifetime with 2% hydrogen.

The unprotected sensors were the first to degrade, where their degradation behaviour is highly similar as shown by the small range in this curve. These sensors

appear to degrade minimally for the first month, at which time they degrade in a roughly linear fashion.

The second sensor to show degradation had the Ballard-type filter, where it appeared to start degrading a month into the test. Again, its early degradation behaviour is roughly linear but with a lower slope than the unfiltered sensors, thus showing that the filter helps. This sensor's behaviour becomes peculiar near the end of the test in that, after dropping to 1.353 V after nearly 4 months, it recovers to 1.469 V by the end of the test. Possible explanations for this behavior are that moisture may have washed away siloxane particles in the filter over time, or perhaps sulfur (what was thought to be D3 siloxane) added to the air in the test at that time chemically reacted with the activated carbon and reduced the siloxane concentration seen by the sensor, thus improving its signal.

The final sensors to show degradation were the RKI-filtered sensors, which appear to increase in signal voltage for the first 2.5 months, when they then begin to show a degradation rate similar to the sensor with the Ballard-supplied filter. Thus, these filters provide complete protection against degradation for 70 days.

Comparing the degradation rate of the unfiltered sensors of Figure 10 with the linear average of a large number of sensors returned from operation in the bus fleet, the test accelerated the degradation by a factor of 15:1. Both RKI protected sensors in the test stayed above the failure degradation amount for about 90 days. This suggests that the average RKI sensor with an RKI filter would begin to see degradation after 2.5 years of operation and would last over 3.5 years.

Figure 11 shows the drop in voltage of the hydrogen sensors, when tested in 2% hydrogen gas from before the test began to after the test was completed. The tests were performed with and without the filters for the sensors that had the filters throughout the test. Note that all of the sensors are degraded at the end of the test (where this test was intentionally extended to see what would happen to the filters as they 'wear out'), but the two unprotected sensors are clearly more heavily degraded than the RKI-filtered sensors and the Ballard-filtered sensor.
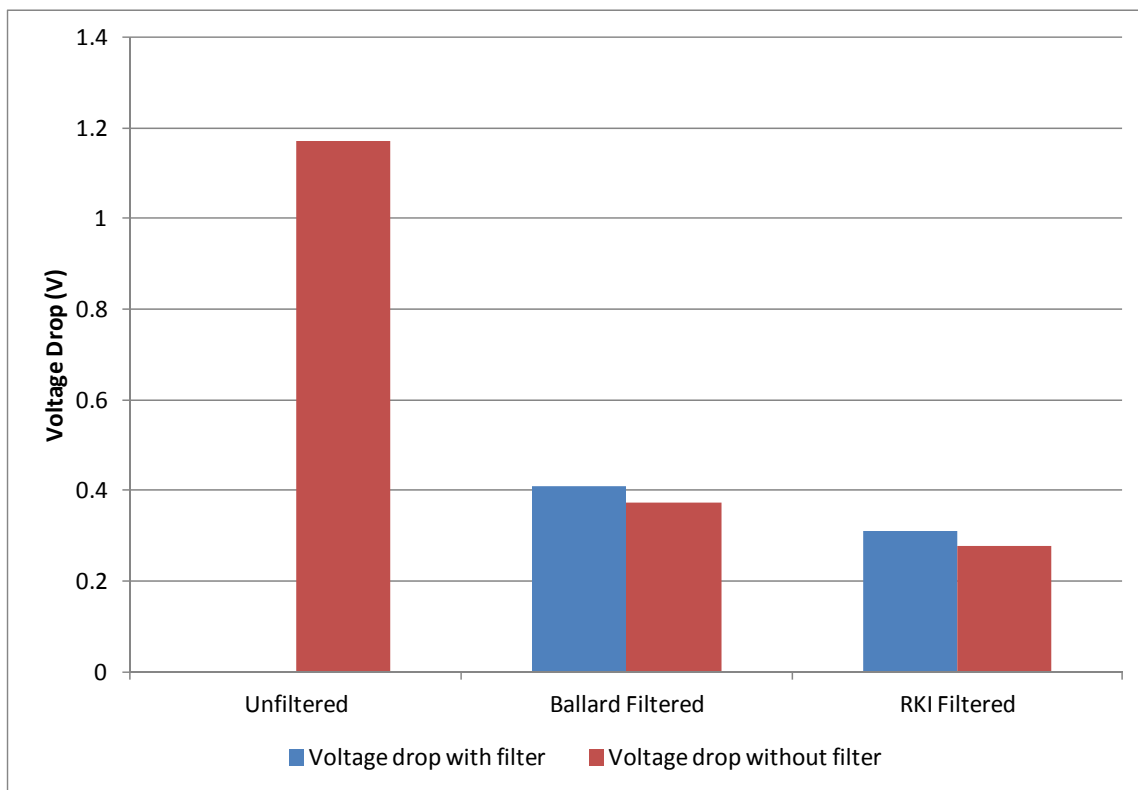
Figure 11 Sensor voltage drop through the test

Figure 11 shows an important detail in the behaviour of the signal voltage-drop through the filters. The results are averaged for the RKI filtered sensors. This figure also shows that part of the degradation observed during the test was actually due to the filters. Not only do the filters reduce the hydrogen signal, they also increase this effect at end of life.

This testing confirmed the ability of the Ballard and RKI-supplied filters to protect the sensors for an extended period. This RKI filter was determined to be much more effective in preventing the siloxane from reaching the sensor bead than the series of prototype filters that Ballard had developed.

3.   In-Situ Calibration

Even in the presence of filtering, the hydrogen sensor voltage drops as the sensor degrades over time. Real time correction of the sensor calibration values was tried using neural networks, as discussed in Appendix A, but did not give consistent results. Another method to compensate for this degradation over time is the implementation of calibration algorithm incorporated in the bus under controlled operating conditions. This calibration technique would ideally be implemented into the regular operating schedule of the bus. This would eliminate the shop time with specialized technicians to recalibrate the sensors. The reference hydrogen concentration for the sensors is calculated from the fuel flows during steady-state operation. Steady state temperature and steady electrical output are required to keep the hydrogen concentration at a constant value. Steady state conditions can be achieved in the bus shortly after start-up before the bus is on route and just prior to shutdown, again when the bus is off route. This chapter discusses the test used to determine if such a method of calibrating the sensors, based on experimental and analytical comparisons, is feasible.

3.1. Sensor Calibration Theory

Conceptually the calibration is performed through a mass balance of the hydrogen flows into and out of the fuel cell anode, as shown in Figure 12. Two to three times the hydrogen required to operate the fuel cell flows through the anode. The hydrogen that is not consumed in the production of electrical energy is recirculated back through the anode. The recirculation entry point is after the hydrogen inlet mass flow meter, so its reading is not affected by the recirculation.

Anode
Fuel Cell

Hydrogen In

Hydrogen consumed to produce electricity
Hydrogen purged to cathode
Hydrogen leak to cathode
Hydrogen leak to environment
Hydrogen crossover to cathode
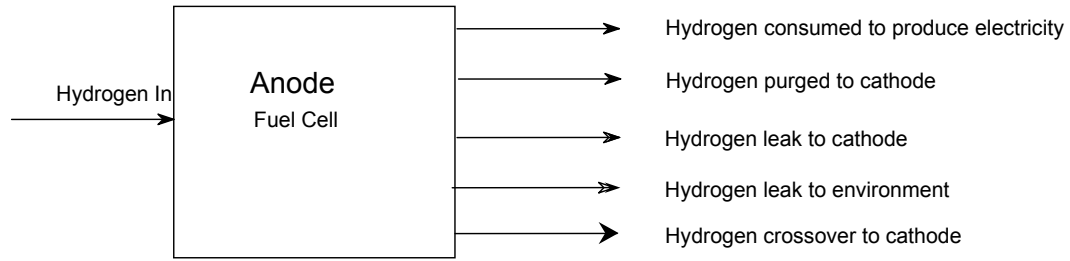
Figure 12 Mass balance of hydrogen flow in a fuel cell anode

Contaminants in the anode flow include water (liquid and gaseous) and nitrogen crossing the membrane from the cathode into the anode. To keep the nitrogen and water contaminants in the anode side to acceptable levels a small quantity of the anode flow is purged to the cathode exhaust. This purge flow includes hydrogen which must be accounted for in the mass balance. With the continuous purge (flow through mode of operation) in this test, the concentration of nitrogen and water in the anode remain low and are ignored. Additionally some of the anode flow leaks to the cathode side, some leaks to the environment, some is permeated through the membrane, and some is consumed in short circuits internal to the fuel cell which are not measured with the ammeter. In low temperature fuel cells these internal shorts are generally small, and can be ignored [18].

The hydrogen concentration in the cathode exhaust is calculated as the flow rate of hydrogen gas in the cathode exhaust divided by the total flow rate, as in Equation (4), where C_{H2} is the cathode exhaust hydrogen concentration, $\dot{n}_{a,out}$ is the flow rate of hydrogen gas exiting the anode of the fuel cell in SLPM and $\dot{n}_{c,out}$ is the flow rate of air exiting the cathode of the fuel cell.

$$C_{H2} = \frac{\dot{n}_{a,out}}{\dot{n}_{c,out} + \dot{n}_{a,out}} \tag{4}$$

Because the tests were done with load, the mass flows exiting the anode and cathode must be known. The outlet flow rates are not measured, and so need to be calculated for the model. The hydrogen purged to the cathode is calculated as the rate of hydrogen into the anode less all the hydrogen flows out of the anode: $\dot{n}_{a,out} = \dot{n}_{a,in} - \dot{n}_{cons} - \dot{n}_{a,perm} - \dot{n}_{l,int} - \dot{n}_{l,ext}$. The cathode outlet flow rate is calculated subtracting the

oxygen consumed for load and recombination of the leaked and permeated hydrogen from the cathode inlet flow rate: $\dot{n}_{c,out} = \dot{n}_{c,in} - \frac{\dot{n}_{cons}+\dot{n}_{a,perm}+\dot{n}_{l,int}+\dot{n}_{l,ext}}{2}$ (see also Equation (9)). The accuracy of the ammeter is +/- 0.1% of reading, so the subtraction of the gas consumed from the inlet flows does not significantly affect the accuracy of the results of the model, Equation (5).

$$C_{H2} = \frac{\dot{n}_{a,in} - \dot{n}_{cons} - \dot{n}_{a,perm} - \dot{n}_{l,int} - \dot{n}_{l,ext}}{\dot{n}_{c,in} - \frac{\dot{n}_{cons} + \dot{n}_{l,int} + \dot{n}_{a,perm} + \dot{n}_{l,ext}}{2} + \dot{n}_{a,in} - \dot{n}_{l,int} - \dot{n}_{a,perm} - \dot{n}_{l,ext} - \dot{n}_{cons}} \qquad \textbf{(5)}$$

The flows shown in Figure 12 and used in Equation (5) are developed below. The reactant consumption is calculated from the load using Faraday's law [19], Equation (6).

$$\dot{n}_x = \frac{I}{nF} \qquad \textbf{(6)}$$

where F is Faraday's constant, $\dot{n}_x$ the amount of reactant consumed in moles per second, n is a reaction specific constant (n=2 for the hydrogen reduction reaction, and n=4 for the oxidation reaction), and I is the current.

The difference in potential between the Nernst voltage and Open Circuit Voltage (OCV) is the result of crossover of fuel and oxidizer through the electrolyte and internal short circuits in the cell. This crossover, also called permeation is determined by Fick's law of diffusion [20], Equation (7).

$$\dot{n}_{a,perm} = -D\frac{\partial C}{\partial x} \qquad \textbf{(7)}$$

Where D is the diffusion coefficient, C is the concentration, and x is the normal direction. The diffusion coefficient and membrane thickness for the PFSA membranes are from the manufacturer's data sheet, shown in Appendix F, and discussed further in Section 3.2.3. The diffusion coefficient given in this appendix was taken at 22° C, 100% RH and is not a routine test. No information is given on the temperature or RH dependence of this coefficient or its reliability. The fuel cell module normally operates at a temperature of about 60° C. Assuming no temperature dependence of the diffusion coefficient of the membrane, 100% RH of the membrane, 100% hydrogen concentration

in the anode, 0% concentration at the cathode side of the membrane, the pressure difference from the anode and cathode side, and using the dimensions of the fuel cell membrane, the diffusion for the test fuel cell is found by Equation (8)

$$\dot{n}_{a,perm} = 0.009\ SLPM$$

<div align="right">(8)</div>

Based on Faraday's law (as well as basic chemical balance equations), the oxygen consumed is half the hydrogen consumed, so the air consumed in the cathode is the summation of the hydrogen consumption rate, internal leak rate, and hydrogen permeation rate, assuming the leak rate is small enough for the hydrogen to completely recombine with oxygen. Equation (9) gives the consumption rate of the cathode flow as:

$$\dot{n}_{c,cons} = \frac{\dot{n}_{cons} + \dot{n}_{l,int} + \dot{n}_{a,perm}}{2}$$

<div align="right">(9)</div>

Referring back to Equation (5), the hydrogen inlet flow is measured, the hydrogen consumed to produce electricity is indirectly measured through the fuel cell electrical current flow, while the hydrogen leak to cathode and the hydrogen leak to the environment are both zero for Section 3.3.1, new membrane testing, but calculated from ex-situ measurements (discussed in Section 3.2.3.1) for the leaky membrane in Section 3.3.2.

Further simplification is achieved by combining the consumption, permeation, and leak terms, each of which acts in a similar way, resulting in the final hydrogen concentration model shown in Equation (10). This calculated concentration is then compared to the RKI sensor measured concentration. The difference between these values is used to determine the degradation level of the RKI sensor and used to determine the amount of degradation in the RKI sensor.

$$C_{H2} = \frac{\dot{n}_{a,in} - \dot{n}_{cons,mod}}{\dot{n}_{c,in} - \frac{3 * \dot{n}_{cons,mod}}{2} + \dot{n}_{a,in}}$$

<div align="right">(10)</div>

3.2. Test Setup

This calibration method was tested in Ballard's lab to prove whether the concept works. The test was implemented on MD05, a manually controlled, 5kW max power test station at Ballard Power Systems, Inc. The fuel cell used in the test setup is a single cell unit, shown in Figure 13. The single cell fuel cell uses prototype hardware with a pressurized rubber balloon to provide the compression required to hold the membrane between the fuel cell end plates. In the figure, the electrode connections are at the top, gas and water supply on the far side, and exhaust on the close side. The green, yellow, and blue hoses are for pressure and the close wires are for thermocouples. The external structure provides the support for the balloon to provide the internal compression.
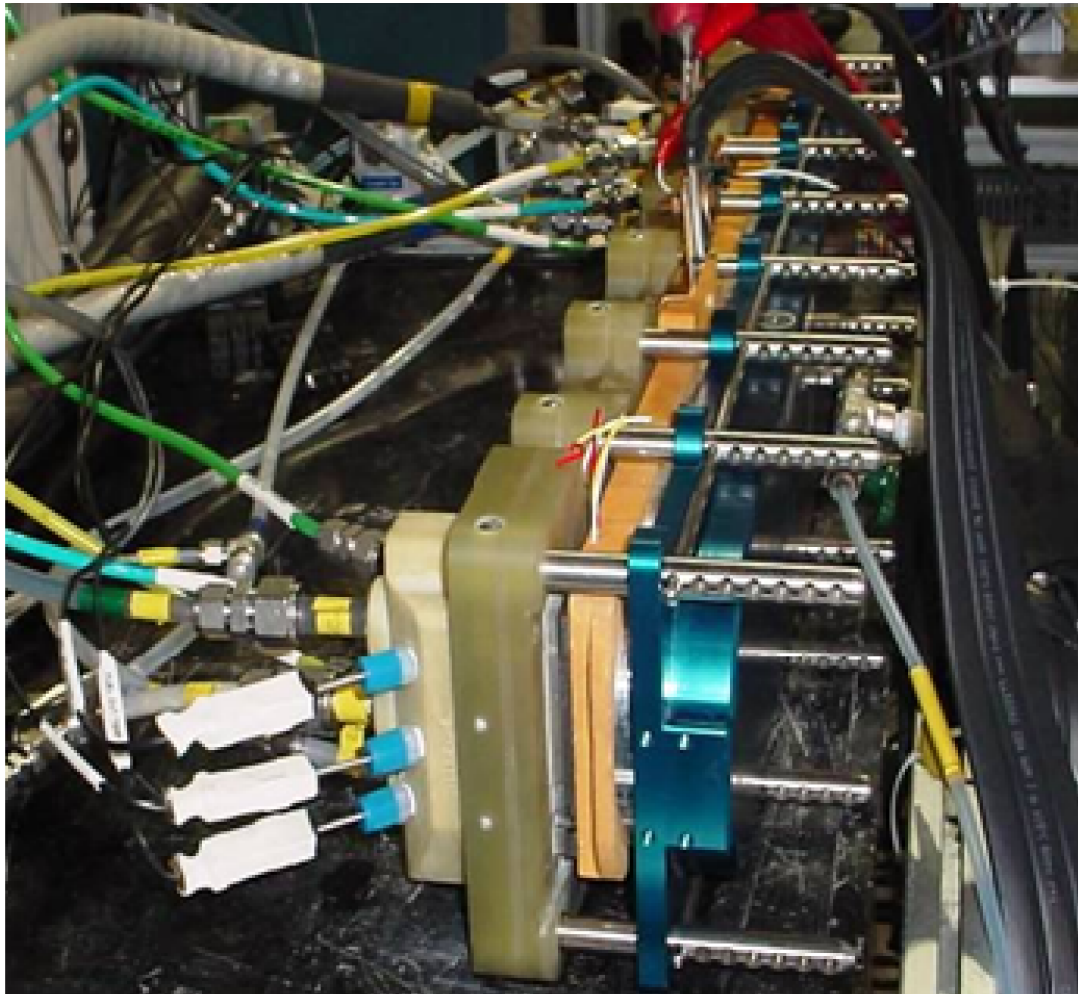
Figure 13 Single cell fuel cell

3.2.1.   Test Station

The test station at MD05 is one commonly used for fuel cell development work. It has the ability to accurately measure gas flows, electrical current produced by the fuel cell and many other characteristic values including operating temperature, gas flow rates and temperatures, etc. Pressurized gasses are supplied to the test station from the facility, and conditioned for the fuel cell. The gasses exit the test station into a building exhaust vent. Water is supplied to the test station to humidify the gasses and cool the fuel cell.

Figure 14 is a simplified diagram of the bus fuel cell and its local peripherals. It is helpful in relating the flows shown in Figure 12 to the fuel cell P&ID shown in Figure 2. This figure shows the anode on the top and the cathode on the bottom of the fuel cell. The gas inlet flow metres are shown in the diagram as $\dot{n}_{a,in}$ and $\dot{n}_{c,in}$, where the subscripts a & c are for anode and cathode respectively. The flow rate $\dot{n}_{cons}$ is the hydrogen consumed in the production of electricity, $\dot{n}_{l,int}$ and $\dot{n}_{l,ext}$ are the leaks, both internal and external, and $\dot{n}_{a,out}$ is the hydrogen flow purged to the cathode. In this figure, the permeation and short circuit hydrogen flows leaving the anode are included in internal leak rate. Additional parameters measured in the HD-6 layout are the anode and cathode inlet and outlet pressures $P_{a,in}$, $P_{a,out}$, $P_{c,in}$, and $P_{c,out}$, and the hydrogen concentration, C_{H_2} as read by the cathode exhaust hydrogen sensor. The HRB is the hydrogen recirculation blower, which continuously recirculates the hydrogen through the anode. The gas leaving the cathode, $\dot{n}_{c,out}$, is the oxygen depleted air which includes the hydrogen leaked from the anode. As noted previously, the leaked hydrogen will combine with oxygen by the catalyst on the cathode side, unless the leak is massive. Such a massive leak is something the hydrogen sensor is used to detect to prevent the cathode from becoming flammable, not something that would be present when calibrating the hydrogen sensor.
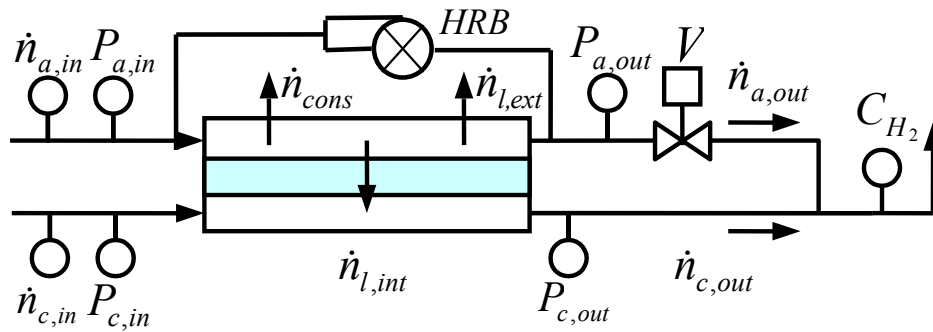
Figure 14 Diagram of HD6 fuel cell and some immediate peripherals

The test setup was simplified to include only the minimum relevant items for the calibration, as shown in Figure 15. The HRB has been removed as hydrogen measurement locations are before and after this system and are thus not affected by the HRB system. The required sensors are the flow rates, which are controlled by Teledyne Model 202 Mass Flow Controllers (MFC's), and which have accuracies of +/- 1% of full scale reading (Appendix G, Appendix H, and Appendix I), and the K&B 12 pressure transducers used to measure the anode and cathode pressures . In Figure 14, V is the purge valve, allowing a periodic purge of the anode loop to remove the nitrogen and water buildup. This the purge valve is not required for the flow through configuration of the test station (Figure 15). The test setup has a manually controlled needle valve on the output of each flow stream to control the pressures.

$$n_{a,in} \qquad\qquad\qquad P$$

$$n_{c,in} \; P_{c,in}$$

Figure 15 Diagram of the experimental setup

Pure hydrogen is humidified and heated and then fed into the anode as shown in Figure 15. Oxygen is obtained from compressed air which is heated and humidified before flowing through the cathode. The humidification of the gaseous streams is required to maintain the humidity of the membrane. The gas pipes feeding the test fuel cell are heated to prevent water condensation before reaching the cell. The coolant pressure, temperature, and flow rate are also controlled by the test station.

After passing through the anode of the fuel cell, the excess hydrogen gas is routed into the cathode outlet piping where it mixes with the exhaust air. This anode purge has a low enough hydrogen flow rate that the concentration in the cathode exhaust is not flammable, and thus can be safely routed through the cathode piping of the test station. The mixture then passes through an aluminum manifold with a mounted hydrogen sensor similar to those used on the busses The hydrogen concentration in this mixture was measured with an RKI FHD-753 hydrogen sensor. The data was acquired with a Chessell 4250M analog data logger, and the signal is logged every 2 seconds with a National Instruments Labview application developed by Ballard.

3.2.2. Reference Sensor Calibrations

To observe how the in-situ calibration method works over the life of a sensor, the test was performed on 3 unfiltered RKI FHD-753 hydrogen sensors at various stages of degradation. A brand new sensor, a partially degraded sensor, and a very degraded\sensor (poor) were calibrated by exposing them to hydrogen on a calibration

station, as per 1.2.2.4.3. The sensitivity of each sensor is shown in Table 2. These sensors are manufactured to have a sensitivity of 1V/%H2, so the recorded sensitivity also shows how good the sensor is relative to a new sensor.

Table 2 Sensitivity in hydrogen sensor calibrations

RKI FHD-753 Hydrogen Sensor	Sensitivity (V/% H2)
Good Sensor (S/N 52090022-3ET)	0.9609
Partially Degraded Sensor (S/N 527016-0029)	0.7877
Poor Sensor (S/N 52090665-25ET)	0.4618

3.2.3.   Membranes

With new technology, membranes have become lighter, thinner, and less expensive. However, while membrane performance and efficiency have improved and cost has decreased, the modifications allow greater transfer of gasses and water through these new thinner membranes. The membrane used in the bus fuel cell modules is made of PFSA, the data sheet for which is shown in Appendix F.

The membrane material is 25.4 microns thick with a hydrogen permeance (crossover flow rate) of < 0.020 $\frac{ml}{min*cm^2}$ at 22C, 100% RH, and 50 psi differential pressure. This membrane, supplied in rolls, has catalyst and gas diffusion fabric layered on each side to make it a membrane electrode assembly (MEA). The single cell fuel cell has only a single membrane. During the testing either one of two MEA's were used. The membrane was either a new bus MEA or one that was removed from a bus fuel cell due to its leaks.

3.2.3.1.   Worn Membrane Leak Characterization

The leak rate for both the new and leaky membranes was tested to provide sufficient data for the internal and external leak rates for the hydrogen concentration model. Both were tested outside of the test station on Ballard's leak test cart to measure the internal and external sealing of the test fuel cells. The internal leak rate of the worn

membrane was then calculated via the experimental results for the new and leaky membranes.

Ballard's leak test cart is used to examine if small fuel cell stacks have leaks, and is often used to ascertain whether the seals have been placed correctly. First, the external leak rate is measured by pressurizing all the cavities of the fuel cell (anode, cathode, and coolant) to 30 psi. After holding the pressure steady, the mass flow meter that feeds the fuel cell gives the flow rate required to maintain the pressure. Neither the single cell with the new MEA nor the one with the leaky MEA showed external leaks when built properly.

Internal leaks are detected by depressurizing the cell and then only pressurizing one chamber in the cell at a time to 7 psi. When the new membrane was installed in the cell, there were no internal leaks. When the worn membrane was in the cell, there was a leak between the anode and cathode, while the coolant chamber was sealed from the anode and cathode.

The simplified equation for the mass balance assumed that all hydrogen that was not consumed to produce electricity was purged to the cathode outlet flow or permeated across the membrane where it was oxidized. For leaky cells, however, the pressure gradient forces hydrogen across the membrane at a much higher rate. This hydrogen is also combined with oxygen to form water at the surface of the cathode side of the membrane. Hence, no extra hydrogen exited the cathode when leaky membrane was used, but the hydrogen purge flow was smaller. This resulted in lower hydrogen concentration at the cathode exhaust sensor compared to the tests with the tests with the new membrane.

The leak rate of the worn membrane, then, is calculated by comparing the cathode hydrogen concentration of the new and leaky membranes. The average difference of the hydrogen outlet flow rates between the membranes is the amount of hydrogen that leaked through the membrane, Equation (11).

$$L = \dot{n}_{a,out,NoLeak} - \dot{n}_{a,out,Leak} = \left(\frac{C_{H2}\dot{n}_{c,out}}{1 - C_{H2}}\right)_{NoLeak} - \left(\frac{C_{H2}\dot{n}_{c,out}}{1 - C_{H2}}\right)_{Leak} \tag{11}$$

The tests with the good sensor show that the internal leak rate of the leaky membrane under the test conditions is 0.089 SLPM.

3.2.4. Test Conditions

The initial test operating conditions were set to mimic bus operating conditions at idle, and adjusted to suit the test station. The flow settings were selected to maintain a hydrogen concentration between 1.0% and 3.5% in the cathode exhaust. The minimum setting is to stay within the controllable flow range of the mass flow meters while the maximum setting is to maintain safety and remain within the range of the RKI hydrogen sensors. To achieve these concentrations, the hydrogen flow rate was set to 0.54, 0.48, 0.40, and 0.35 SLPM during testing, while the air flow rate was set at 10 SLPM and the electrical load was set to 25 Amps.

Initially, a mixer was intended to be used to supply the anode with a hydrogen/nitrogen mixture, increasing the total anode flow rate while maintaining a high enough hydrogen flow rate and low enough outlet hydrogen concentration. This would have allowed higher flow rates in the anode and maintained a more uniform differential pressure between the anode and cathode throughout the anode flow channels. As the mixer was not functioning properly, the anode flow was limited to pure hydrogen at a much lower total anode flow rate. At this flow rate, the pressure drop through the anode is minimal while the cathode maintained a normal pressure drop, so at the outlet of the fuel cell the differential pressure between the anode and the cathode is significantly larger than at the inlet. Since permeation is not a function of pressure and the leak in the worn membrane is at the inlet, this change does not significantly affect the results.

The temperature of the fuel cell was kept at 58°C during testing, the air inlet temperature at 66°C, and the fuel inlet temperature 38°C. The fuel temperature dropped 8°C between the test station and the anode inlet due to heat loss in the plumbing. The low flow rate makes it difficult for the gas to maintain its temperature before it reaches the fuel cell, even with insulated and heated pipes.

The anode and cathode inlet pressures were set at 7.0 psi and 6.6 psi respectively. This differential pressure was set lower than the normal 2-3 psi differential to bring the average differential pressure across the membrane closer to the bus

operating condition, due to the low anode flow rate. However the average differential pressure (dP) is still higher than in a bus. As most of the hydrogen leakage is near the inlet flow, the lower inlet anode pressure reduced hydrogen leakage flow across the good membrane. It also brought the leakage rate from the leaky membrane to manageable levels, since its leak was close to the inlet. With the low hydrogen flow and normal air flow, the differential pressure increased significantly through the fuel cell.

Each of the flows for the model in Equation (10) are presented in Table 3, along with the accuracies of each measurement. All three of the sensors were testes at each of the flow rates in the table below for both membranes. More testing will improve the accuracy of these parameters.

Table 3 Variables in hydrogen concentration equation

Variable	Magnitude	Accuracy	Variable Description
$\dot{n}_{c,in}$	10 SLPM	1%	Inlet air flow rate
$\dot{n}_{a,in}$	0.35, 0.40, 0.48, 0.54 SLPM	1%	Inlet hydrogen flow rates
$\dot{n}_{cons}$	0.17 SLPM	0.1%	Hydrogen consumed for load
$\dot{n}_{a,perm}$	<0.009 SLPM	50%*	Hydrogen permeated to cathode
$\dot{n}_{l,int}$	0, 0.089 SLPM	10%*	Hydrogen leaked to cathode (good and leaky membranes)
$\dot{n}_{l,ext}$	0.003 SLPM	50%*	Hydrogen leaked to environment
$\dot{n}_{cons,mod}$	0.18 SLPM	+0.1% -2.6%*	Combination of consumption and permeation
$\dot{n}_{cons,mod,l}$	0.27 SLPM	+3.5% -5%**	Combined consumption, internal leak, and permeation

*estimated accuracy, **estimated, combined internal leak and permeation

3.2.5. Test Procedure

The first test was with the good sensor and the new membrane. The good sensor was installed on the manifold in the cathode exhaust, and the new membrane was installed in the test fixture between two endplates. The test station was turned on and started up according to Ballard procedures. The gas and cooling flows were selected according to the test conditions above, starting with the high hydrogen flow rate. Before the first test run, the test station was allowed to operate for 30 minutes until hygrothermal equilibrium was reached and pressure and temperature readings became steady-state. After a measurement was taken over five minutes with the results averaged at the high flow rate, the hydrogen flow was reduced to the next condition. At this condition the back pressure valves were adjusted to maintain the same pressure conditions at the inlet, and the fuel cell was allowed to reach steady state before the next measurement is taken. This approach was repeated for each hydrogen flow rate.

Figure 16 is a graph of the raw data from the new sensor tested with the new membrane. Each stepwise change in hydrogen inlet flow rate (pink) in the graph indicates the hydrogen flow being adjusted to one of the four settings. Thus, the data for all four flow rates was collected continuously, and are presented on the same graph. The fuel consumed (turquoise), electrical load (light blue), and air inlet flow rate (dark blue) remained constant for each of the hydrogen flow rates. After steady state was achieved, data was collected for 5 minutes and the average of the hydrogen flow rate, oxygen flow rate, load, and cathode exhaust hydrogen concentration (red) readings were taken. The first three values are used to calculate the expected hydrogen concentration from Equation (10), and are compared with the measured hydrogen concentration.
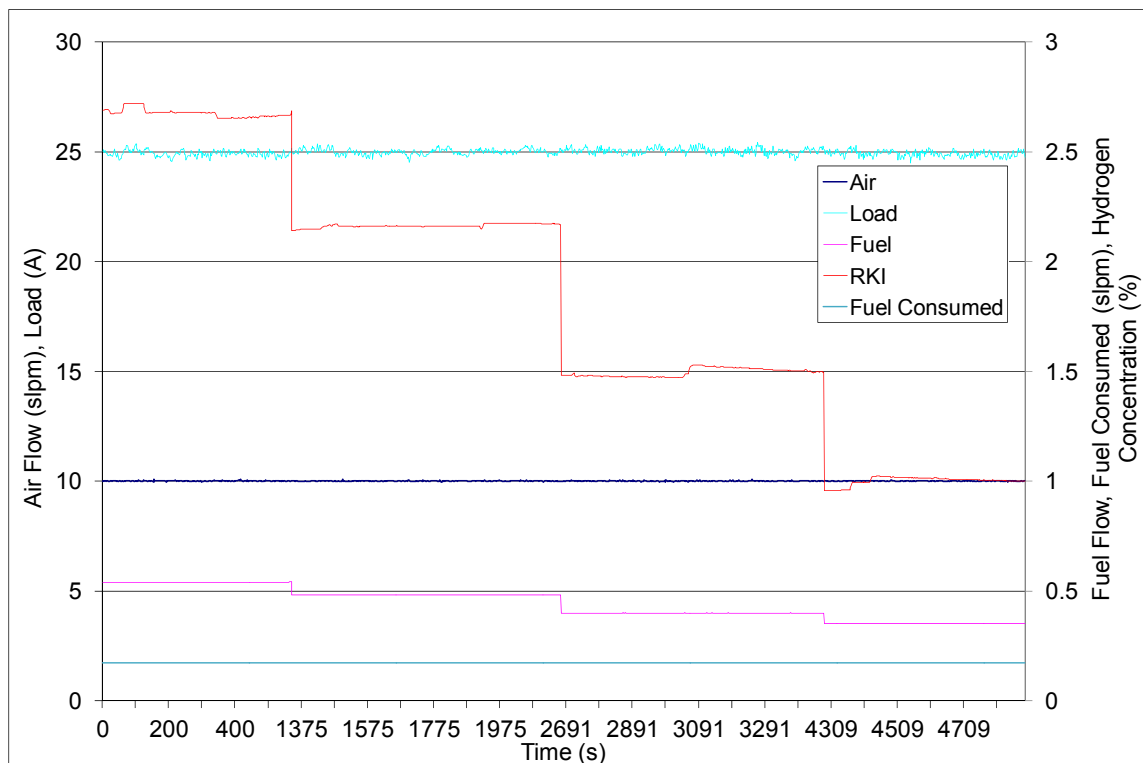
Figure 16 Sample experimental measurements required for the model

During each new hydrogen flow rate, the hydrogen back-pressure valve had to be adjusted to maintain inlet pressure. The station was allowed 10 minutes at each flow rate to stabilize with slight adjustments to manually controlled valves to maintain conditions as constant as possible. This is visible in the RKI measurement at the third flow rate (2690-4300s) of Figure 16, when the anode back-pressure valve was initially closed too tightly, resulting in a slow filling of the anode and a restriction on the purged hydrogen, and, thus, a slightly lower hydrogen concentration reading. This was corrected by slightly opening the anode back-pressure valve, resulting in a blip in the RKI sensor reading as the anode pressure dropped to its proper level and hydrogen evacuating the anode increased the RKI reading on the graph. The flow rate was considered steady state once the anode pressure remained constant.

After the good sensor was tested, the MD05 test station shut down procedure was followed and the partially degraded sensor was installed. The station was started up again, and in this way the partially degraded and the poor sensors were tested. This

entire test procedure was repeated for each of the test conditions discussed in Section 3.2.4.

3.3. Experimental Results

In operation, the fuel cell just described with a constant flow purge valve had the hydrogen flowing into the cathode exhaust from the anode, mixing with the air to create a steady hydrogen concentration. Continuous data was collected for the duration of the test. In post-processing this data, the five minutes of steady operation at each of the flow rates was identified, and the average hydrogen concentration from the mass balance was compared with the hydrogen sensor reading. The same data was also analyzed for the partially degraded and poor sensors and the good and leaky membrane with the results shown below.

The results for the three sensors indicate also that with further testing, a resistance value for the diffusion of hydrogen the silicone dioxide could be calculated. Further testing would have to be done to calculate the other parts of Fick's law of diffusion, but this would be useful for future studies.

3.3.1. Results from New PEM Membrane

Figure 17 shows the hydrogen concentration vs. flow rate from the results. The hydrogen concentration calculated from the flow results ($\dot{n}_{a,in}$, $\dot{n}_{c,in}$, and C_{H2} in Figure 15) is calculated using the simplified model given in Equation 10 and shown as expected value. The measurement of each of the good, partially degraded, and poor sensors using calibration values for new sensors are also shown
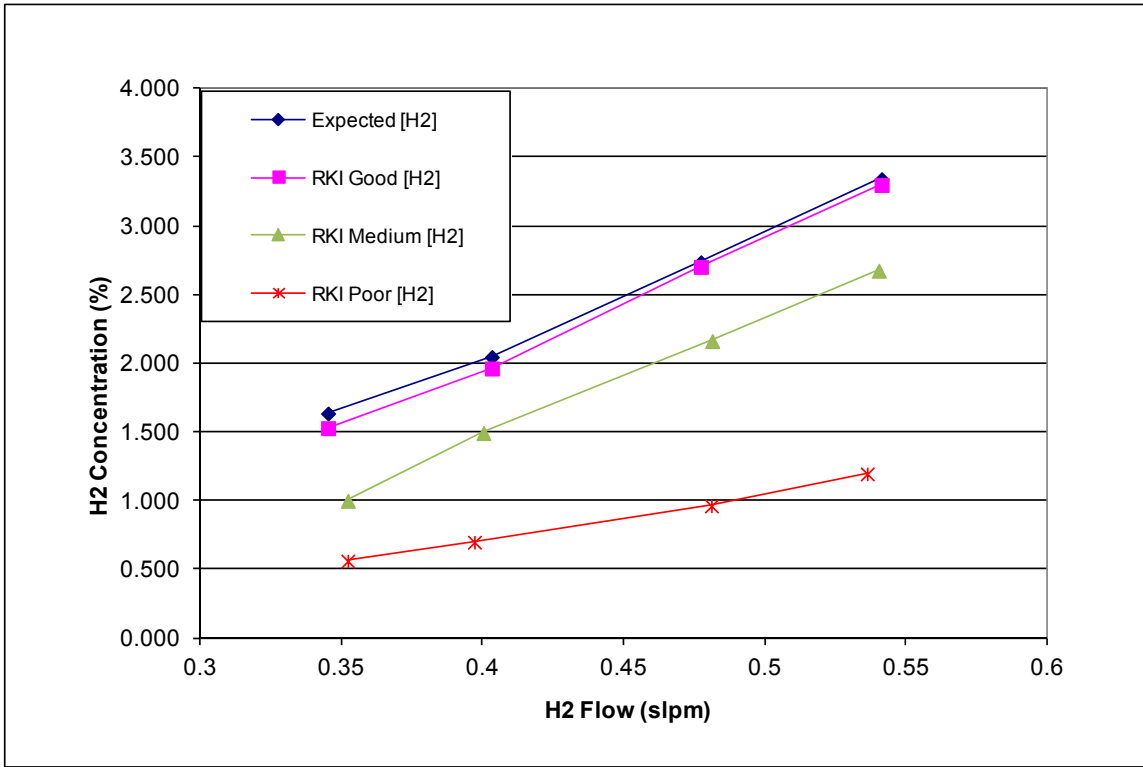
***Figure 17 Different measures of Hydrogen concentration vs. hydrogen flow rate
from test with new membrane.***

Linear regression was performed on each of the lines in Figure 17, and each

showed the x-intercept, as expected, to approximate the value of $\dot{n}_{cons,mod}$, 0.18 SLPM.

The slope of each sensor is then compared with the expected concentration to calibrate

the sensitivities of the sensors, with the x-intercept set to $\dot{n}_{cons,mod} = 0.180\ SLPM$. Table

4 compares the sensitivities measured ex-situ (Section 1.2.2.4.3) with the sensitivities

calculated from in-situ measurements from this experiment. More detailed results are in

Appendix J.

Table 4 Hydrogen sensor calibrations with the new membrane

RKI FHD-752 Hydrogen Sensor	Sensitivity (V/% H2) Ex-Situ Calibration	Sensitivity (V/% H2) In-Situ Calibration	Percent Error of In-Situ Calibration
Good Sensor	0.9609	0.977	1.7%
Partially Degraded Sensor	0.7877	0.758	-3.4%
Poor Sensor	0.4618	0.353	-23.6%

As seen from Table 4, the in-situ calibration method works very well for sensors that are not degraded when the membrane is new. As the sensors degrade more and the signal becomes farther from the expected value, the in-situ calibration suggests that the sensors are more degraded than they actually are. This error is small for the partially degraded sensor but appreciable for the poor sensor. With the poor sensor, in-situ calibration will result in the sensor reading a higher hydrogen concentration than the actual concentration. Although this may produce false positive readings of flammable concentrations of hydrogen, it will not give false negative readings, keeping the module safe. The other positive factor is that the larger than necessary change in calibration factor will result in the sensor being replaced sooner.

3.3.2. Results from Leaky PEM Membrane

The same test was repeated with the MEA with the leak. The average of the good, partially degraded, and poor RKI sensor readings are plotted in Figure 18 with the estimation of the hydrogen concentration calculated for the leaky membrane from the model (Equation (10)).
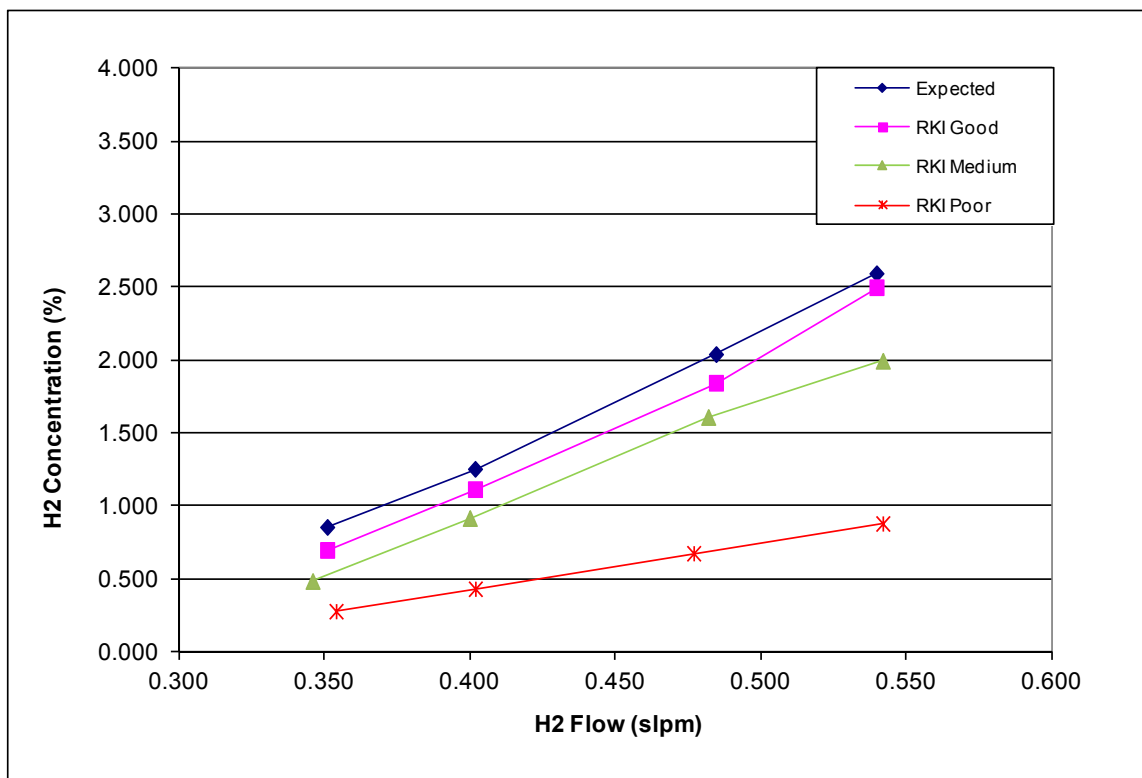
Figure 18 Estimation of hydrogen concentration vs. hydrogen sensor measurement from test with leaky membrane.

The linear regression performed on this data showed the x-intercept, as expected, to approximate the value of $\dot{n}_{cons,mod}$ for the leaky cell, 0.27 SLPM. The slope of each sensor is then compared with the expected concentration to calibrate the sensitivities of the sensors, with the x-intercept locked on $\dot{n}_{cons,mod}$. Table 4 compares the sensitivities measured ex-situ with the sensitivities calculated from in-situ measurements. More detailed results for this condition are in Appendix J.

Table 5 Hydrogen sensor calibrations

RKI FHD-752 Hydrogen Sensor	Sensitivity (V/% H2) Ex-Situ Calibration	Sensitivity (V/% H2) In-Situ Calibration	Percent Error of In-Situ Calibration
Good Sensor	0.9609	0.914	-4.8%
Partially Degraded Sensor	0.7877	0.754	-4.2%
Poor Sensor	0.4618	0.337	-27.0%

As seen from Table 5, the in-situ calibration method works very well for sensors that are slightly or not degraded, even in a leaky cell, if the leak rate is known. The

results with the degraded sensors are similar to the results with a good membrane with similar conclusions.

3.4. Sensitivity Analysis

The calibration model should be accurate and robust, meaning that small errors in measured mass flows, current flow, or in any of the unmeasured leakage rates should not cause a large error in the sensor calibration. The model should be accurate enough that the estimate of hydrogen concentration can be used to reliably detect degraded sensors. This robustness checking is performed through sensitivity analysis. The sensitivity will also show the sensitivity at the different flow rates, indicating at which flow rate the most accurate calibration can be performed.

Many types of sensitivity analysis exist. One-At-a-Time (OAT) analysis checks the sensitivity on one input variable at a time. This sensitivity analysis technique was selected as the data collected in this test lends itself to OAT analysis. However, only sensitivity for a particular variable can be found from each variable. To find the overall sensitivity of the model using OAT analysis, the different partial derivatives need to be combined with a norm. A 3-D graph (Figure 19) of the model (Equation (10)) shows that the model is nearly planar in the region of interest (the same is true for the operating conditions of the bus), and, hence, the norm should be the 1-norm or taxicab norm. The taxicab norm is the sum of the magnitudes of the derivatives.
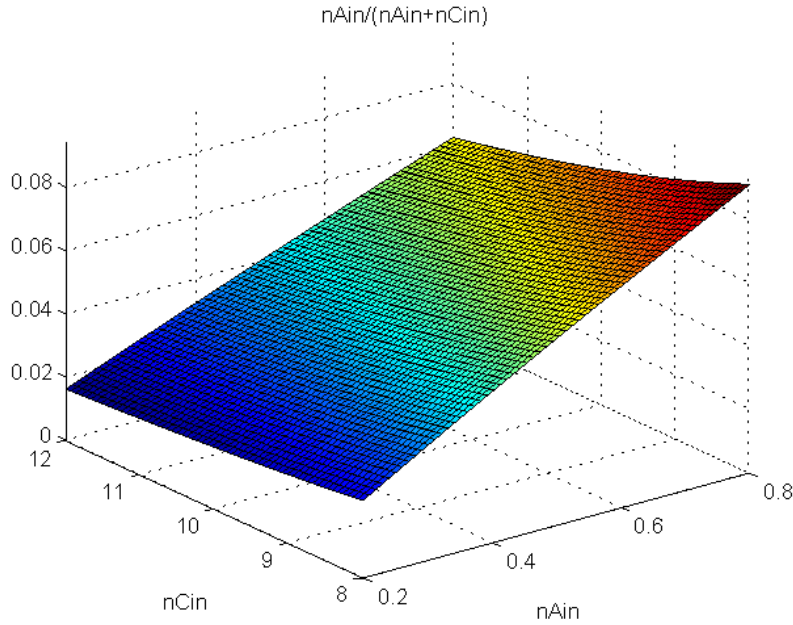
Figure 19 Surface plot of hydrogen concentration versus flow rates

The OAT analysis is performed by taking the partial derivatives of the model (Equation (10)) with respect to the major gas flow rates ($\dot{n}_{a,in}$, $\dot{n}_{c,in}$, and $\dot{n}_{cons,mod}$ ($\dot{n}_{cons,mod,l}$ for the leaky membrane)) with the results shown in Equation (12), Equation (13), and Equation (14). The accuracy of each of the model inputs is used to calculate the respective differentials. These values are divided by the expected hydrogen concentration to give the sensitivity of the model output as a percentage. The accuracy of the model is, then, the sum of the derivatives (Equation (15), Equation (16)). The magnitude and accuracy of each of the derivatives in the model and the differentials is shown in Table 3. The $\partial \dot{n}$ terms are given in the accuracy column of this table.

3.4.1.   Sensitivity Analysis for New Membrane

For a new membrane, the outlet flows are more accurate than with a leaky membrane. The partial derivatives and the final sensitivity equations are shown below.

$$\frac{\partial C_{H2}}{\partial \dot{n}_{a,in}} = \frac{\dot{n}_{c,in} - \frac{\dot{n}_{cons,mod}}{2}}{(\dot{n}_{c,in} + \dot{n}_{a,in} - \frac{3\dot{n}_{cons,mod}}{2})^2} \qquad (12)$$

47

$$\frac{\partial C_{H2}}{\partial \dot{n}_{c,in}} = -\frac{\dot{n}_{a,in} - \dot{n}_{cons,mod}}{(\dot{n}_{c,in} + \dot{n}_{a,in} - \frac{3\dot{n}_{cons,mod}}{2})^2}$$

$$(13)$$

$$\frac{\partial C_{H2}}{\partial \dot{n}_{cons,mod}} = -\frac{\dot{n}_{c,in} - \frac{\dot{n}_{a,in}}{2}}{(\dot{n}_{c,in} + \dot{n}_{a,in} - \frac{3\dot{n}_{cons,mod}}{2})^2}$$

$$(14)$$

$$\frac{dC_{H2}}{C_{H2}} = \left(\frac{\dot{n}_{c,in} - \frac{\dot{n}_{cons,mod}}{2}}{\left(\dot{n}_{c,in} + \dot{n}_{a,in} - \frac{3\dot{n}_{cons,mod}}{2}\right)^2} \partial \dot{n}_{a,in}\right.$$
$$+ \frac{\dot{n}_{a,in} - \dot{n}_{cons,mod}}{\left(\dot{n}_{c,in} + \dot{n}_{a,in} - \frac{3\dot{n}_{cons,mod}}{2}\right)^2} \partial \dot{n}_{c,in}$$
$$\left. + \frac{\dot{n}_{c,in} - \frac{\dot{n}_{a,in}}{2}}{\left(\dot{n}_{c,in} + \dot{n}_{a,in} - \frac{3\dot{n}_{cons,mod}}{2}\right)^2} \partial \dot{n}_{cons,mod}\right)/C_{H2}$$

$$(15)$$

A summary of the sensitivity results is shown in Table 6. The cathode flow has the biggest component of model error, while the error due to anode flow is also quite significant, but decreases as the hydrogen flow rate increases. Thus, the higher the hydrogen concentration, the better the accuracy of the estimated hydrogen concentration relative to hydrogen flow rate. The load and permeation add minimal error to the model.

Table 6 Sensitivity analysis of model for new membrane

Anode inlet flow rate	Accuracy w.r.t. anode flow	Accuracy w.r.t. cathode flow	Accuracy w.r.t load/permeation	Accuracy - combined
0.35	17.3%	11.9%	0.0%	29.3%
0.40	13.3%	11.8%	0.0%	25.2%

0.48	9.7%	11.8%	0.0%	21.5%
0.54	8.0%	11.7%	0.0%	19.8%

In this range the accuracy of the expected hydrogen concentration is very similar, the higher the hydrogen concentration, the better the accuracy of the estimated hydrogen concentration relative to hydrogen flow rate, though the magnitude of error can increase.

Figure 20 shows the combined accuracy of the model from Table 6 plotted alongside the accuracy of the sensors. The good sensor is nearly identical to the model value, while the degraded sensors using the calibration of a new sensor show that they do not fall inside of the error bars of the modeled hydrogen concentration, so this method of calibration can be used to reliably detect degraded hydrogen sensors.
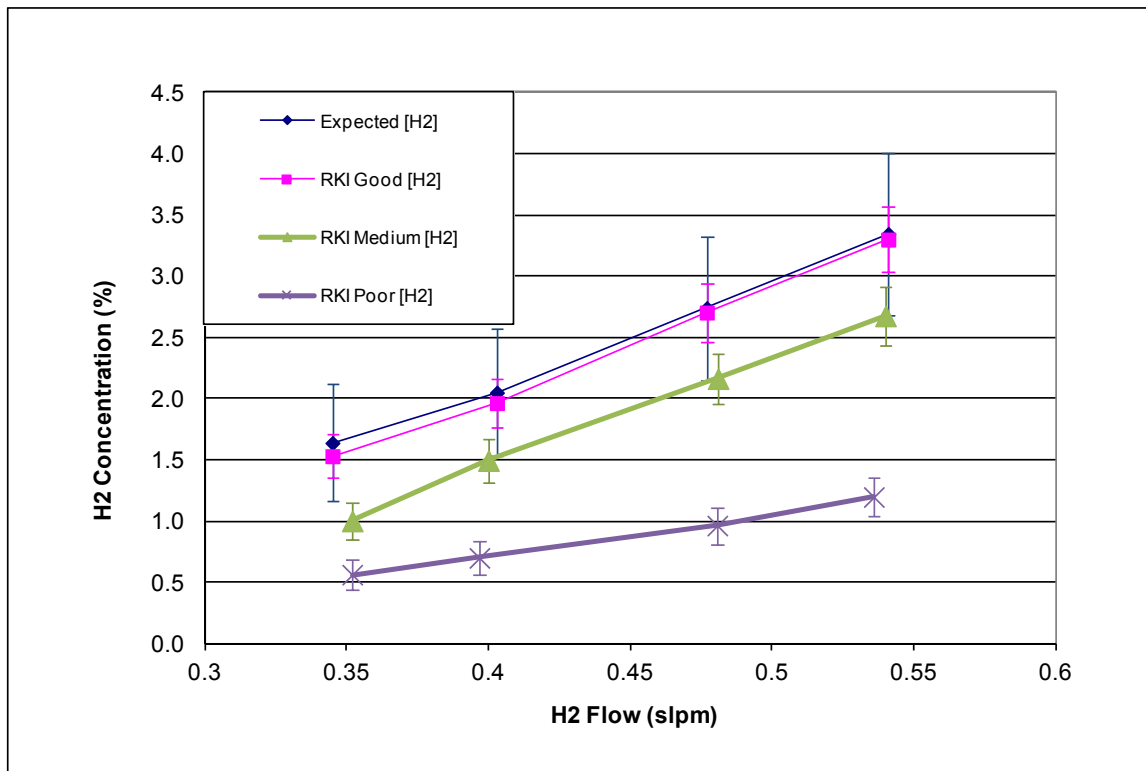
Figure 20 Effect of hydrogen and air flow error on hydrogen concentration estimate for the new membrane

3.4.2. Sensitivity Analysis for Leaky Membrane

Sensitivity analysis was also conducted on the results from the leaky membrane. Leaky membranes have lower flow certainty due to uncertainty in leak rate. The equations for the leaky membrane sensitivity analysis are the same as for the new membrane, but $\dot{n}_{cons,mod}$ is replaced with $\dot{n}_{cons,mod,l}$ in Equation (15) for the accuracy to give Equation (16).

$$\frac{dC_{H2}}{C_{H2}} = (\frac{\dot{n}_{c,in} - \frac{\dot{n}_{cons,mod,l}}{2}}{\left(\dot{n}_{c,in} + \dot{n}_{a,in} - \frac{3\dot{n}_{cons,mod,l}}{2}\right)^2} \partial \dot{n}_{a,in}$$

$$+ \frac{\dot{n}_{a,in} - \dot{n}_{cons,mod,l}}{\left(\dot{n}_{c,in} + \dot{n}_{a,in} - \frac{3\dot{n}_{cons,mod,l}}{2}\right)^2} \partial \dot{n}_{c,in} \qquad \textbf{(16)}$$

$$+ \frac{\dot{n}_{c,in} - \frac{\dot{n}_{a,in}}{2}}{\left(\dot{n}_{c,in} + \dot{n}_{a,in} - \frac{3\dot{n}_{cons,mod,l}}{2}\right)^2} \partial \dot{n}_{cons,mod,l})/C_{H2}$$

Table 7 shows the results of the sensitivity analysis of the data from the leaky membrane. As the anode flow rate increases, the accuracy with respect to the anode flow rate and with respect to load/leak improves greatly, while there is only slight improvement in the accuracy with respect to the cathode flow rate, though more than there is with the new membrane.

Table 7 Sensitivity analysis of model with leak

Anode inlet flow rate	Accuracy w.r.t. anode flow	Accuracy w.r.t. cathode flow rate	Accuracy w.r.t. load/leak	Accuracy - combined
0.35	37.2	12.1%	11.7%	60.9%
0.40	22.8	12.0%	7.1%	41.9%
0.48	14.0%	11.9%	4.4%	30.3%
0.54	10.8%	11.8%	3.4%	26.0%

Figure 21 shows the combined accuracy on the modeled hydrogen concentration and on the model compensated for the known leak rate. The RKI measurement error bars reflect the manufacturer specified accuracy for a new sensor, while the error bars for the expected hydrogen flow are calculated from the sensitivity analysis. The partially degraded sensor reading is within the error bars for the expected reading. This show that a sensor that is considered "failed" could not reliably be shown as failed with the leaky membrane.
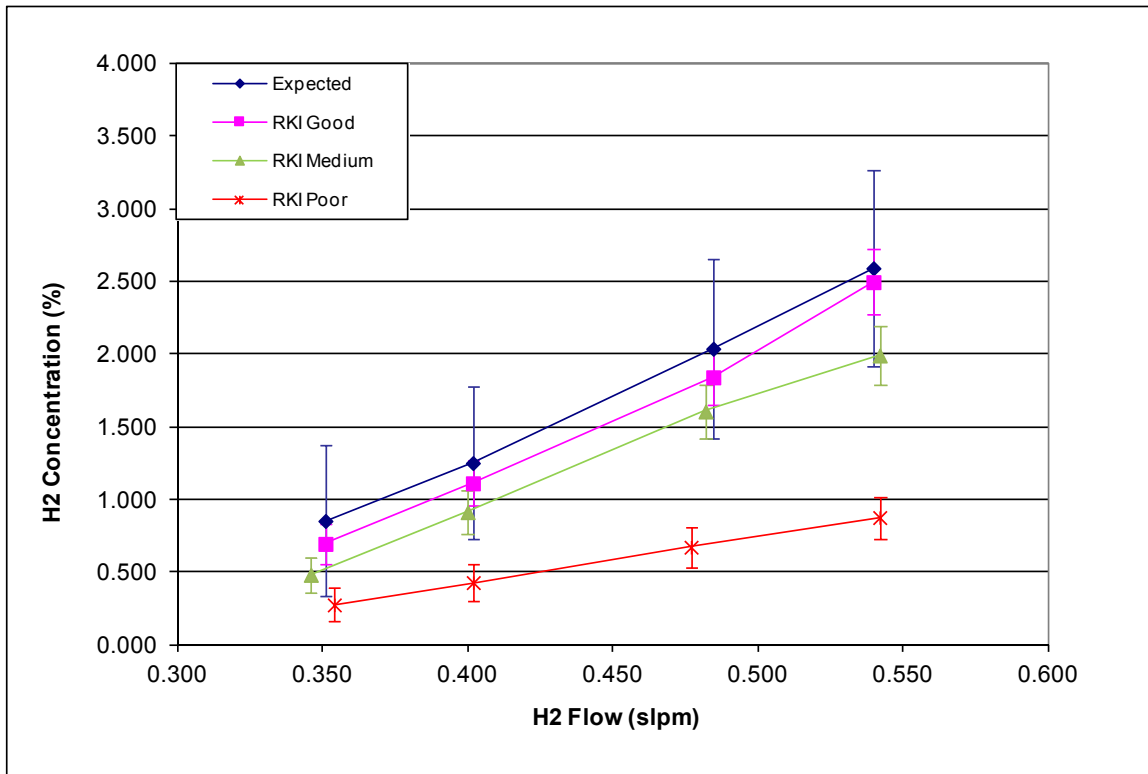
Figure 21 Effect of hydrogen and air flow error on hydrogen concentration for the leaky membrane

The good RKI sensor reading with its accuracy is shown Figure 22. The model modified for a leaky membrane gives a good estimation of the hydrogen concentration, as measured by the good sensor. The hydrogen concentration, as estimated assuming no leak, is shown in the top line in Figure 22. This shows that the effect of leak on hydrogen flow rate is significant enough that the hydrogen concentration model must take the leak into account.
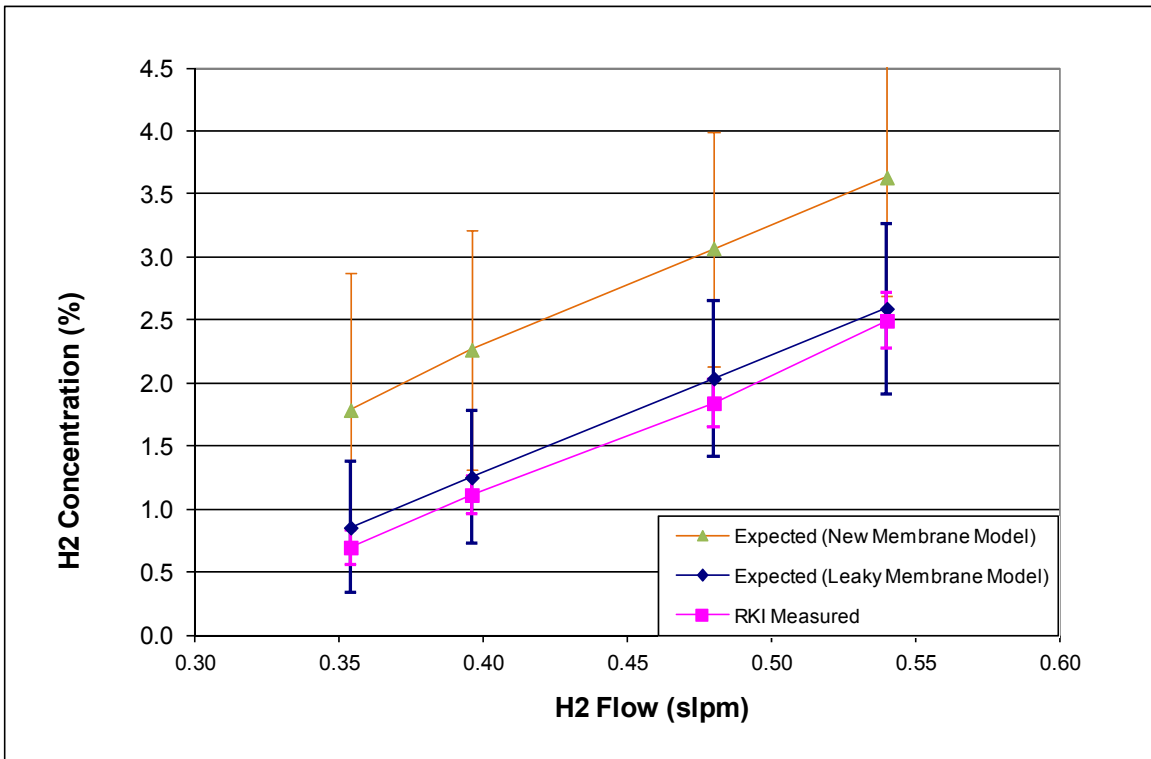
Figure 22 Expected hydrogen concentration from new membrane model and leaky membrane model compared with good RKI sensor reading

4. Conclusions

This paper has examined two different methods for extending the lifetimes of catalytic-type hydrogen sensors used in the cathode exhaust of PEM fuel cells. The first method involved the development of physical filtering. Activated carbon filters were developed and fitted over the sensor to capture the siloxanes, preventing them from coalescing on the surface of the hydrogen sensor catalytic beads and forming silicates. This physical filtering slows the degradation rate of the sensors significantly (as shown in an accelerated test comparing filtered and unfiltered sensors in Figure 10), but does not eliminate degradation entirely.

There is evidence in the measurements to suspect that the activated carbon filters work extremely well at the beginning of their life, and degrade over time. For this reason time based filter replacement is recommended as a preventative maintenance strategy. Ideally a replacement interval for the filters can be found to give the sensors infinite life.

To further extend sensor life, further work has been done to examine the possibility of developing an in-situ calibration algorithm based on measured input fuel and air flows, the consumption of fuel by stack current, and known leak rate. A model was developed to calculate the expected cathode exhaust hydrogen concentration for a stack whose excess fuel flow is continuously purged to the cathode exhaust. The model is expected to work equally well with a stack utilizing the HRB. This model, when compared to cathode hydrogen sensor measurements made with good and degraded hydrogen sensors in a single-cell proof-of-concept test (see Figure 17), shows good agreement with the cathode exhaust concentration measured with the good sensor, and shows that the degraded sensors are reading low. As indicated in Table 5, this initial test shows that the model can be used to accurately estimate the sensitivity of the good and slightly degraded sensors, but overestimates the degradation of significantly-degraded sensors for a fuel cell with a non-leaky membrane.

A sensitivity analysis examining the effect of variations in measured input fuel and air flows, and consumption plus leaked flow on exhaust hydrogen concentration was performed. This sensitivity analysis (see Table 6 and Table 7) shows that the cathode flow carries the biggest component of model error, followed by the error due to anode flow; but this decreases as the hydrogen flow rate increases. Thus, in the test fuel cell, higher hydrogen flow rates result in better accuracy of the estimated hydrogen concentration relative to hydrogen flow rate. The load and permeation, as well-defined and small parameters respectively, add minimal error to the model.

Application of this sensitivity model to a single-cell test with a membrane that has a transfer and including this leak in the model (see RKI Expected, Compensated in Figure 22) results in a situation of more uncertainty, but the model still gives generally good agreement in predicting close to the measured hydrogen concentrations with the good sensor. This finding (with about a third or more of the fuel consumed being leaked across the membrane) suggests that, in some future use of the model for in-situ calibration of the cathode exhaust sensor, as long as the fuel flow lost through transfers is small or included in the model, the model can be used to detect and/or re-calibrate degraded sensors with acceptable accuracy.

This proof-of-concept model and testing illustrates that, through the use of fuel flow and air flow monitoring during steady state operation (and possibly some ongoing estimate of transfer or crossover leak flow) the cathode exhaust hydrogen concentration can be predicted very well in the test fuel cell. Although more work is required before a detailed algorithm can be developed for in-situ sensor calibration in the HD6 module, the results are promising enough that it should be pursued.

If the model in the bus is not robust enough for sensor calibration in busses, it can also be used as a diagnostic tool to alert the service providers that the cathode sensor is degraded and requires service.

A path to in-situ calibration using the change in observed exhaust hydrogen concentration when purging to the cathode exhaust versus not purging has also been identified.

5. Modifications for Next Generation Fuel Cell Module

This section describes modifications that will make the techniques discussed in this thesis easier to implement in a working fuel cell. The current generation of fuel cells does not incorporate fuel flow monitoring, though it does have an air flow metre. Neither are small leaks measured. The anode purge cycle currently used in the HD6 module on a timed basis results in transients in the cathode exhaust hydrogen concentration, preventing steady-state measurements. Each of these is required to implement the in-situ hydrogen sensor calibration method described in this thesis.

Fuel flow monitoring is planned to be implemented via a dP gauge across an orifice plate in the hydrogen supply line. This orifice provides the additional advantage of being a restriction to limit the hydrogen flow, should a massive leak develop downstream from the flow meter.

Small leak measurement is not essential early in the fuel cell life for this method of leak detection to work, but will give increased accuracy. Later in the fuel cell life as leaks become bigger, the leak measurement becomes essential. Current research at Ballard is investigating several methods to characterize leaks, including a fuel flow monitoring method.

Another prerequisite is steady-state cathode exhaust hydrogen concentration while the calibration occurs. This will be implemented by using a constantly partially open proportional width modulated valve to control the flow rate to allow constant purging. This would keep a constant concentration of H2 in the anode as well as reduce the strain on the system due to transients.

The model used in this analysis will need to be extended to include the mass flow of water vapour. In the test fuel cell the water vapour in the cathode exhaust due to water production from the reaction is ignored in the Equation (10) model, as the

hydrogen sensor is a significant distance downstream of the fuel cell, and, in the test setup, the temperature of the gasses has cooled to room temperature such that the water vapour has mostly condensed. Ignoring the vapour in the cathode outlet adds an inaccuracy of the calculated hydrogen concentration of less than 5%, assuming a temperature of approximately 303K. Although in the bus the cathode exhaust concentration sensor is a similar distance from the fuel cell, the flow rates are much higher and the piping is all contained in the fuel cell module, which may provide a warmer environment. This causes the gas temperature to be considerably higher with less time for condensation. Consequently, for this method to be implemented in the bus program, the vapour would have to be taken into account.

References

[1] Mench, M. M., Fuel Cell Engines, John Wiley and Sons, Hoboken, 2008

[2] CRC Handbook of Chemistry and Physics, 87th ed, 2006-2007; p 16-13. http://www.hbcpnetbase.com (Accessed February 1, 2014).

[1] Mench, M. M., Fuel Cell Engines, John Wiley and Sons, Hoboken, 2008

[2] CRC Handbook of Chemistry and Physics, 87th ed, 2006-2007; p 16-13. http://www.hbcpnetbase.com (Accessed February 1, 2014).

[3] Ahluwalia, R. K., Wang, X., Buildup of nitrogen in direct hydrogen polymer-electrolyte fuel cell stacks. Journal of Power Sources, Vol. 171, pp. 63-71 (2007)

[4] FCvelocity™-HD6 Integration Manual, Ballard Internal Document, MAN5100204 0H, 22 March 2011.

[5] Yuan, X., Wang, H., Sun, J.C., Zhang, J., AC impedance technique in PEM fuel cell diagnosis—A review, International Journal of Hydrogen Energy,32 (2007) 4365 – 4380

[6] Ramschak,E., Peinecke, V., Prenninger,P., Schaffer,T., Hacker, V., Detection of fuel cell critical status by stack voltage analysis, Journal of Power Sources 157 (2006) 837–840

[7] Mousa, G., Golnaraghi, F., DeVaal, J., Young, A., Detecting proton exchange membrane fuel cell hydrogen leak using electrochemical impedance spectroscopy method, J. of Power Sources, 246 (2014) 110-116

[8] G. Tian, S. Wasterlain, I. Endichi, D. Candusso, F. Harel, X. Francios, et al., J. Power Sources 182 (2008) 449-61

[9] L. Boon-Brett, J. Bousek, G. Black, P. Moretto, P. Castello, T. Hubert, U. Banach, Identifying performance gaps in hydrogen safety sensor technology for automotive and stationary applications, International Journal of Hydrogen Energy 35 (2010) 373–384

[10] L. Boon-Brett, J. Bousek, P. Moretto, Reliability of commercially available hydrogen sensors for detection of hydrogen at critical concentrations: Part II – selected sensor test results, International Journal of Hydrogen Energy 34 (2009) 562–571

[11] Mor, G.K.1; Varghese, O.K.1; Paulose, M.1; Grimes, C.A., A self-cleaning, room-temperature titania-nanotube hydrogen gas sensor, Source: Sensor Letters, v 1, n 1, 42-6, Dec. 2003

[12] Hughes, K.L., Miller, S.L., Rodrigues, J.L., McWorter, P.J., Calibration of an integrated hydrogen gas-sensing system, Sensors and Actuators B, (1996) 75-81

[13] Alag, S., Agogino, A. M., and Morjaria, M., A Methodology For Intelligent Sensor Measurement, Validation, Fusion, And Fault Detection For Equipment Monitoring And Diagnostics, Artificial Intelligence for Engineering Design, Analysis and Manufacturing, vol. 15, pp. 307-320 (2001)

[14] Tsujita, W., Ishida, H., Moriizumi, T., Dynamic Gas Sensor Network for Air Pollution Monitoring and Its Auto-Calibration, Proceedings of IEEE, Sensors, Vol. 1, pp. 24-27 (2004)

[15] Ketler, A. E., Baker, B. H., Narayanan, T., Sargent, L. E., Smathers, R. C., Graber, E. R. (2004). U.S. Patent No. 0055359. Washington, DC: U.S. Patent and Trademark Office.

[16] Osowski, S., Linh, T. H., and Brudzewski, K., Neuro-Fuzzy TSK Network for Calibration of Semiconductor Sensor Array for Gas Measurements, IEEE Transactions On Instrumentation And Measurement, Vol. 53, No. 3 (2004)

[17] Alag, S., Agogino, A. M., and Morjaria, M., A methodology for intelligent sensor measurement, validation, fusion, and fault detection for equipment monitoring and diagnostics, Artificial Intelligence for Engineering Design, Analysis and Manufacturing, Vol. 15, pp. 307-320. (2001)

[18] Mench, M. M., Fuel Cell Engines, John Wiley and Sons, Hoboken, 2008, p 175

[19] Mench, M. M., Fuel Cell Engines, John Wiley and Sons, Hoboken, 2008, p 45

[20] Bird, R. B., Stewart, W. E., and Lightfoot, E. N., "Transport Phenomena", 2nd ed.,Wiley, New York, 2002.

Appendices

Appendix A.

Neural Network Approach

Because the sensors degrade with time/usage, it would be nice to fit a simple equation to the degradation curve to find out the remaining lifetime of the sensors to go from time based preventative maintenance to predictive maintenance. If the sensitivity can be accurately estimated by this equation, the useful lifetime of the sensors could be lengthened by adjusting the calibration of the sensor. However, due to the large variation in the rate of degradation between sensors, even when the degradation is normalized, this is impossible. To overcome the variability in degradation, artificial intelligence techniques were used to attempt to extract either the sensitivity of the sensor or the actual concentration of hydrogen in the cathode exhaust using ANFIS, a utility in MATLAB which stands for Adaptive Neuro Fuzzy Inference Systems.

ANFIS Theory

Perhaps the greatest advantage of Adaptive Neural Networks (ANN's) is their ability to be used as an arbitrary function approximation mechanism that 'learns' from observed data.

An ANN is typically defined by three types of parameters:

1. The interconnection pattern between different layers of neurons
2. The learning process for updating the weights of the interconnections
3. The activation function that converts a neuron's weighted input to its output activation.

If the neural network model, learning algorithm, and activation function are selected appropriately, the resulting ANN can be extremely robust in system identification.

A neuro-fuzzy network is an ANN with a Fuzzy Inference System (FIS) in the body of the ANN. Depending on the FIS type, there are several layers that simulate the processes involved in a fuzzy inference such as fuzzification, inference, aggregation and

61

defuzzification. Embedding an FIS in a general structure of an ANN has the benefit of using available ANN training methods to find the parameters of the fuzzy system.

Methods

The objective of this approach was to allow the hydrogen sensors to be used even in the presence of degradation. Hence, the actual hydrogen concentration as well as the level of degradation of the sensor were needed. Two approaches are available using ANFIS to achieve this.

- Directly use the intelligent system to estimate the concentration. The degradation level is the difference between measured and estimated concentration

- Determine the degradation of the sensor using ANFIS. The actual hydrogen concentration is the measured value with this correction factor applied

To provide the training data for the ANFIS model, operating data was downloaded from two busses in Whistler. During the lifetime of a sensor in a module, it is calibrated ex-situ several times. The data for ANFIS training was taken from the operating data near the calibration events.

For the first method, the ex-situ calibration is used to correct the sensor readings, and these corrected values are used as the target for the ANFIS training. For the second method, the ex-situ calibrations themselves are used as the target.

This model is tested by inputting another data set where the calibration is known and determining how the model performs

Data Sets

Ballard keeps track of the operating conditions of the fuel cell in each of the buses they power around the world. Each data set includes date and time, voltage, load,

time the module has been in operation, air inlet pressure, hydrogen inlet and outlet pressures, cathode exhaust H2 concentration, when the anode purge valve is open and closed, the calibration of the cathode exhaust sensor for each data set, and the cathode exhaust hydrogen concentration corrected for the sensor calibration. Sets of this data from sensors recorded from Whistler buses 2008 and 2021 were used.

The sensor signal for bus 2021 is shown in Figure 23. Each block of data from near one of the calibration events is separated by a red vertical line. This signal was used in all the training while each of the other pieces of data was used optionally for the best training regime.
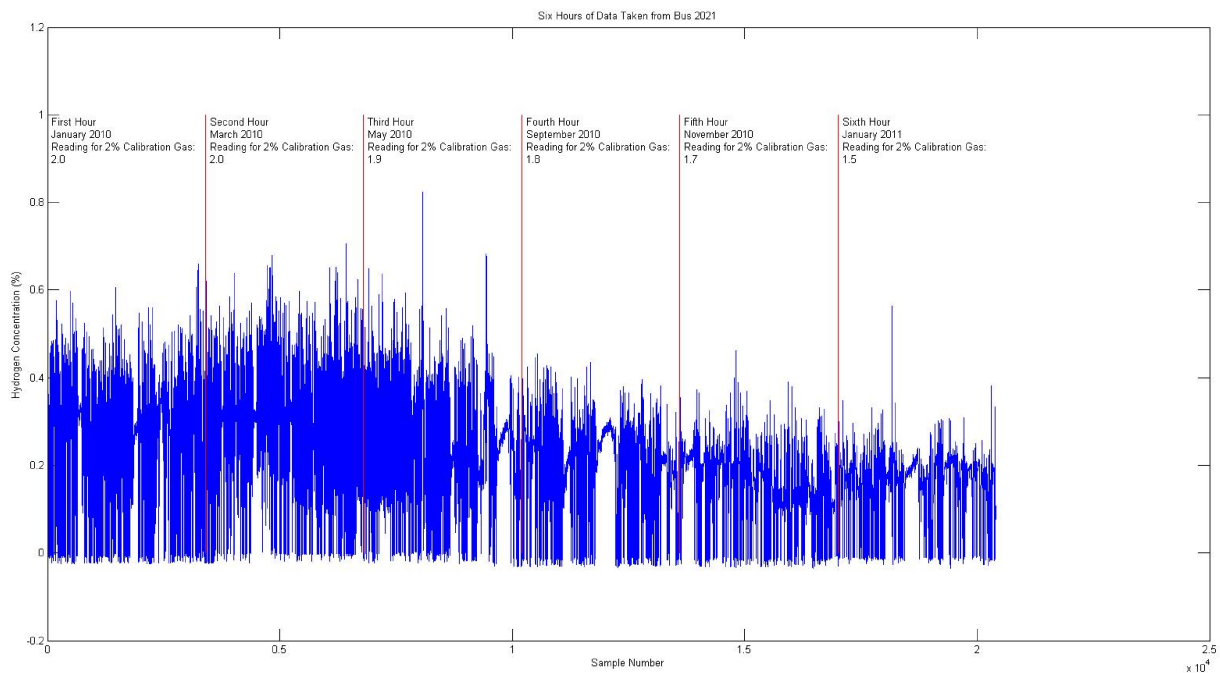
Figure 23 Sensor data for bus 2021 for six one-hour periods

Creating an ANFIS Model on Sensor Degradation Test Data

The Matlab code used to create and run the model is shown in Appendix B. The model uses the default number of layers and 7 membership functions. More layers and membership functions was more costly in processing and time with no improvement. Fewer layers and membership functions was less accurate

63

Estimate Sensor Output

This method uses ANFIS to directly estimate H2 concentration dynamically. The target is the corrected hydrogen exhaust concentration. This method did not show consistent results.

Estimate Sensor Sensitivity

When the calibration of the sensor was used as the target in the ANFIS training, the results were used to estimate the sensitivity of the sensor and use that to correct the sensor readings. This worked for bus 2021 data, but the model for that bus does not work for other buses.

Confine Input to a Specific Current

It was thought that the ANFIS model might work better if one of the environment variables was held constant and the dynamics removed by calibrating at a specific constant current.

The analysis based on electrical load has so far proved the best, using only the hydrogen sensor and module current (scaled to match the hydrogen sensor readings more closely).

Conclusions

Real time correction of the sensor values was tried and has been discussed in this Appendix. Two separate techniques were attempted which involved measurements over the life of the fuel cell. While good results were obtained for the fuel cell in the bus used for the measurements, it was found that the results were fuel cell specific. The sensor calibration model was tried on data collected from a fuel cell in another bus and the sensor calibration model did not work.

Appendix B.

ANFIS Code

```matlab
%%%%%%%%%%%%%%%%%%%%%%%%%%%%%%%%%%%%%%%%%%%%%%%%%%%%%%%%%%%%%%%%%%%%%%%%
%%%%%%%%%%%%%%%%%%%%%%%%%%%%%%%%%%%%%%
% Fuzzy Inference system for estimating hydrogen concentration from a
bus
% sensor. This program loads a MAT file of data downloaded at specific
% times
%
% Daniel Zwart
% Simon Fraser University
% 2012


close all
clear all
% load Bus2021
% load BothBusses
load Bus2021Current
Current=2; % 2 - 20, 4 - 40, 6 - 50, 8 - 70, 10 - 245, 11 - 250
b=.01:0.01:1;
a=sum(b);
% CT_1_2=filter(b,a,CT_1_2);
% AT_J5_2=filter(b,a,AT_J5_2);
eval(['DateTime_' num2str(Current) '=DateTime_' num2str(Current)
'/(DateTime(2)-DateTime(1));'])
eval(['data1 = [DateTime_' num2str(Current) ' SOV_H1_' num2str(Current)
'  AT_J1_' num2str(Current) '  AT_J5_' num2str(Current) '  CT_1_'
num2str(Current) ' HOURS_' num2str(Current) ' PT_A2_' num2str(Current)
' PT_H2_' num2str(Current) ' PT_H3_' num2str(Current) ' VT_HV1_'
num2str(Current) ' AT_J5_TARGET_' num2str(Current) ' CalTarg_'
num2str(Current) ' ];'])
clear SO* AT* CT_1 HO* PT* VT*
% load ..\..\Bus2008\v2\Bus2008
% DateTime=DateTime/(DateTime(2)-DateTime(1));
% data2 = [DateTime SOV_H1 AT_J1 AT_J5 CT_1 HOURS PT_A2 PT_H2 PT_H3
VT_HV1 AT_J5_TARGET CalTarg];
% clear Da* SO* AT* CT_1 HO* PT* VT*


% data2 = [DateTime SOV_H1 AT_J5 CT_1 AT_J5_TARGET];


x1 = [data1(:,5)/300 data1(:,4)];% data1(:,2)];% data1(:,7)
data1(:,10)];
y1 = data1(:,11);
y1 = filter(b,a,data1(:,11));
y1 = data1(:,12);
trnData1 = [x1 y1];
```

```matlab
tstData1 = [x1];

numMFs = [5];
mfType = 'gbellmf';
epoch_n = 20;
in_fis = genfis1(trnData1,numMFs,mfType);
out_fis = anfis(trnData1,in_fis,epoch_n);

[output1, IRR, ORR, ARR]= evalfis(tstData1,out_fis);
figure
plot(y1)
hold on
plot(output1, 'r')
plot(data1(:,4), 'c')
% a=line([3601 3600], [1 0]);
% set(a,'Color',[1,0,0])
% b=line([3001+3601 3001+3601], [1 0]);
% set(b,'Color',[1,0,0])
% c=line([3001*2+3601 3001*2+3601], [1 0]);
% set(c,'Color',[1,0,0])
% d=line([3001*2+3601*2 3001*2+3601*2], [1 0]);
% set(d,'Color',[1,0,0])
% e=line([3001*2+3601*3 3001*2+3601*3], [1 0]);
% set(e,'Color',[1,0,0])
legend('Target Data','ANFIS Output','Training2');
title('ANFIS Results for Training Data (Bus 2021)')
xlabel('Time (s)')
ylabel('Hydrogen Concentration (%)')

% [output2, IRR2, ORR2, ARR2]= evalfis(tstData2,out_fis);
% figure
% plot(z2)
% hold on
% plot(output2, 'r')
% plot(data2(:,4), 'c')
% g=line([3600 3600], [1 0]);
% set(g,'Color',[1,0,0])
% h=line([3600*2 3600*2], [1 0]);
% set(h,'Color',[1,0,0])
% j=line([3600*3 3600*3], [1 0]);
% set(j,'Color',[1,0,0])
% k=line([3600*4 3600*4], [1 0]);
% set(k,'Color',[1,0,0])
% m=line([3600*5 3600*5], [1 0]);
% set(m,'Color',[1,0,0])
% legend('Target Data','ANFIS Output','Training2');
% title('ANFIS Results for Data from Other Bus (Bus 2008)');
% xlabel('Time (s)')
% ylabel('Hydrogen Concentration (%)')
```

Appendix C.

Data Sheet for RKI 752 Hydrogen Sensors

H2 concentration - Output voltage
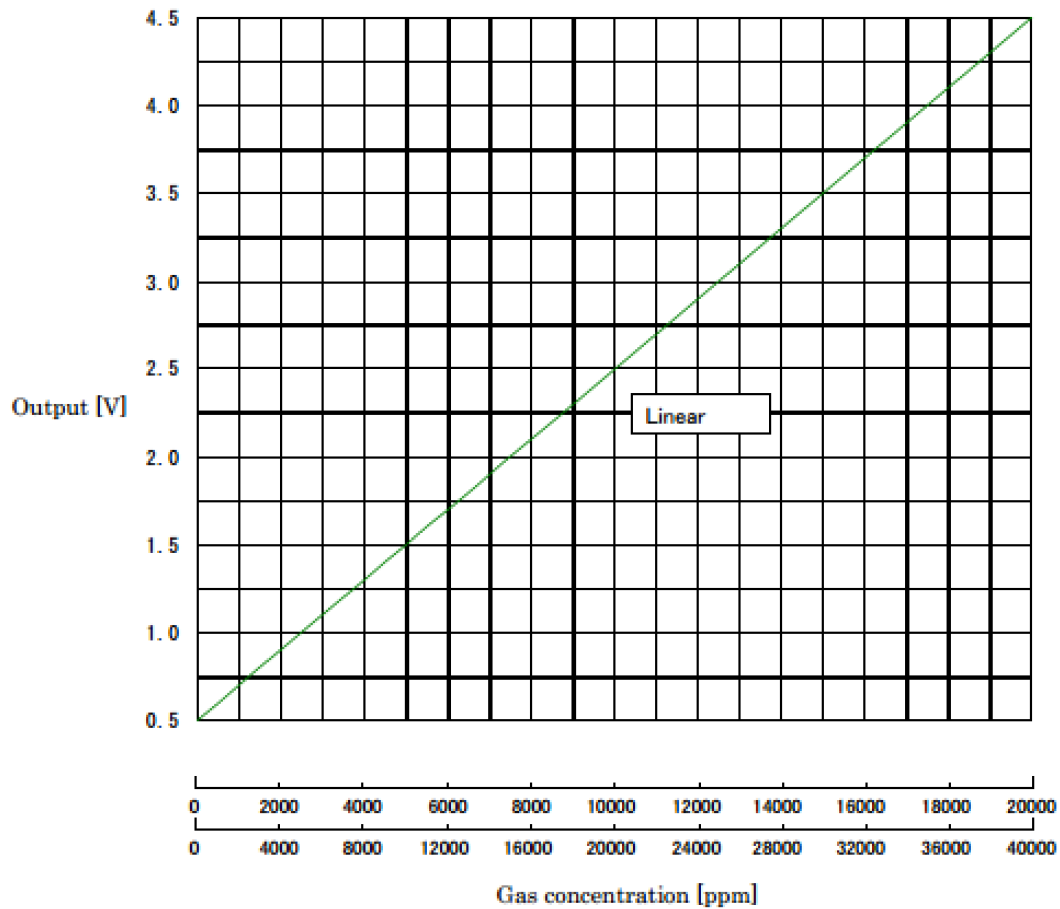
Initial accuracy of FHD·752

Initial accuracy for each H2 concentration is listed below.

0 ppm	+/- 1000 ppm
10000 ppm	+/- 1500 ppm
30000 ppm	+/- 3000 ppm

Appendix D.

Technical Specifications for NTM SenseH$_2$

NTM Sensors
We sense a Green future™

Table of Typical Characteristics:

Metric	Min	Max	Units
Characteristics:			
H$_2$ range (in air)	0.25	4.0	%
Voltage input	12	24	Vdc
Output (sensing range)	1.0	4.5	Vdc
Error state (output signal)	0.0	0.75	Vdc
Error state (output signal)	4.75	5.00	Vdc
Power consumption (25 C)	0.10	0.15	A
Response time (T90)	—	5	Sec.
Recovery time (T10)	—	5	Sec.
Environmental Conditions:			
Ambient temperature	-20	80	C
Relative humidity	5	95	%R.H.
Hazardous Location Approvals:	UL Class I, Div 2, GR C, T2B ATEX Class I, Zone 2 AEx nA IIC, T2		

Typical Calibration:
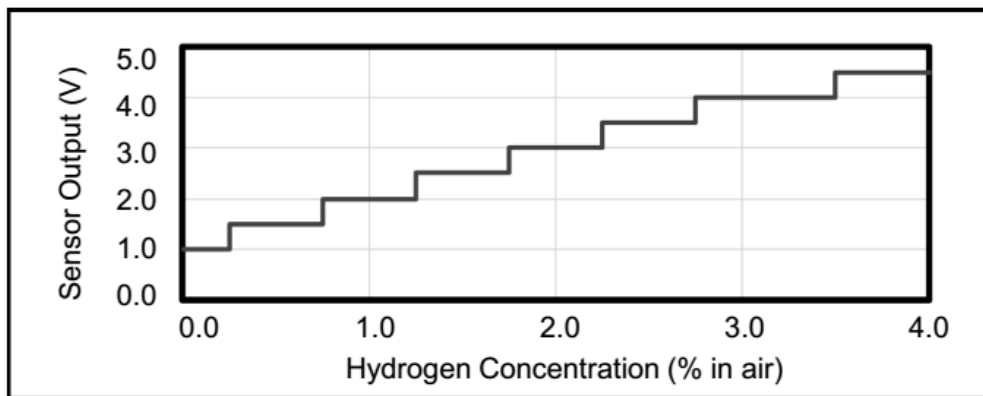
Intended Uses:

- The NTM SenseH$_2$™ is intended for use as a hydrogen gas detector in the range of 0.25 to 4% hydrogen in air.
- Typical applications include: Stationary fuel cells, Fuel cell powered forklift trucks, Hydrogen refueling stations, Hydrogen generation (electrolyzer) systems, On-site fuel reforming systems, Uninterruptible power supply (UPS) systems monitoring, Telecom systems monitoring, or Laboratory monitoring.

Appendix E.

RKI Filter Installation

K10051   Mounting instruction of charcoal filter   Riken Keiki co.,ltd.

1.Part

| Charcoal filter | Teflon filter | Filter cap |
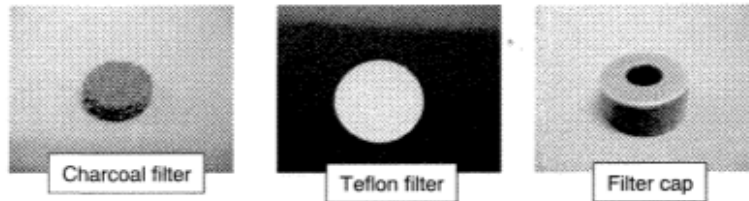
2.Mounting instruction

(1)Charcoal filter is putted on the region of contact.
  (Ref. the fig.1 and fig.2)
(2)Teflon filter is putted on the charcoal filter.
  (Ref. the fig.3)
(3)Filter cap is firmly anchored in detector.
  (Ref. the fig.4)

Filter cap
Teflon filter
FHD-752
Charcoal filter

断面図

Fig.1   Fig.2

Fig.3   Fig.4
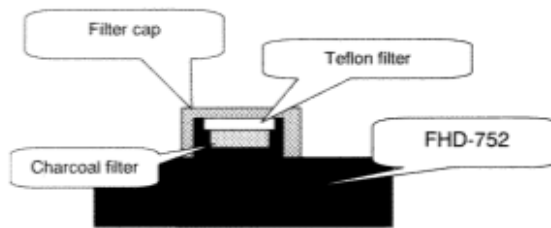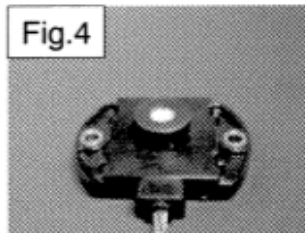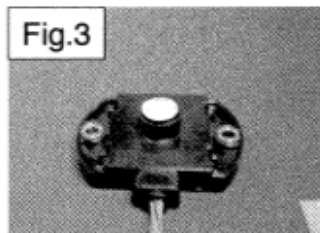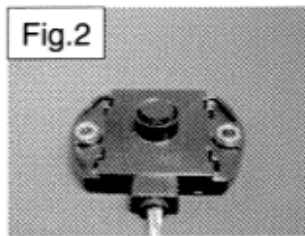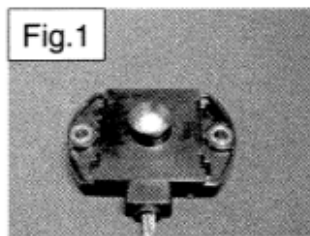
Appendix F.

Data for the membrane from the data sheet

Commercially-available perfluorosulfonic acid (PFSA) membrane

Thickness 25 mm

Hydrogen Crossover < 0.020 ms/min/cm^2

Tested at 22C, 100% RH, and 50 psi pressure differential

Other data withheld due to confidentiality

Appendix G.

Teledyne Hastings Type 202 Mass Flow Controller Data Sheet

1.3 Specifications HFC-202*

Accuracy[1] and Linearity	±1% F.S.
Repeatability	±0.05% F.S.
Std Pressure Rating	500 psig
High Pressure Option	Proof tested to 1500 psig
Pressure Coefficient	-0.0067%/psi (0 - 1000 psig N2) typical
Control Valve DP*	per customer order
Leak Integrity	< 1×10^9 sccs
Temperature Coefficient 3	Zero ±0.035% FS/°C (0 - 60°C)
	Span ±0.05% RDG/°C (0 - 60°C)
STP	0°C and 760 Torr
Power (±15 Volt controller)	±(14 - 16) VDC @ +60 mA/-185 mA (< 3 Watts)
Power (24 Volt controller)	(14 - 32) VDC < 4.2 Watts
Flow Signal	(inherently linear) 0 - 5.00 VDC or 4 - 20 mA
Command Signal	0 - 5.00 VDC or 4 - 20 mA
Wetted Material[2]	316 SS, 302 SS, Nickel, Viton,
	82/18 Au/Ni Braze, Trace Silver Solder, Kalrez®
Connector	15-pin subminiature D / (9-pinfor 24 Volt)
Fittings	¼ in Swagelok, others available
Weight (approx)	1.8 lb (0.82 kg)

1 Stated accuracy is for nitrogen or other gas specific calibration and using this gas only.

2 Other materials are available. Viton is the standard O-ring option.

* Specifications may vary for instruments with ranges greater than 10 SLPM.

Page 5 of Teledyne Hastings Instruments Instruction Manual

Appendix H.

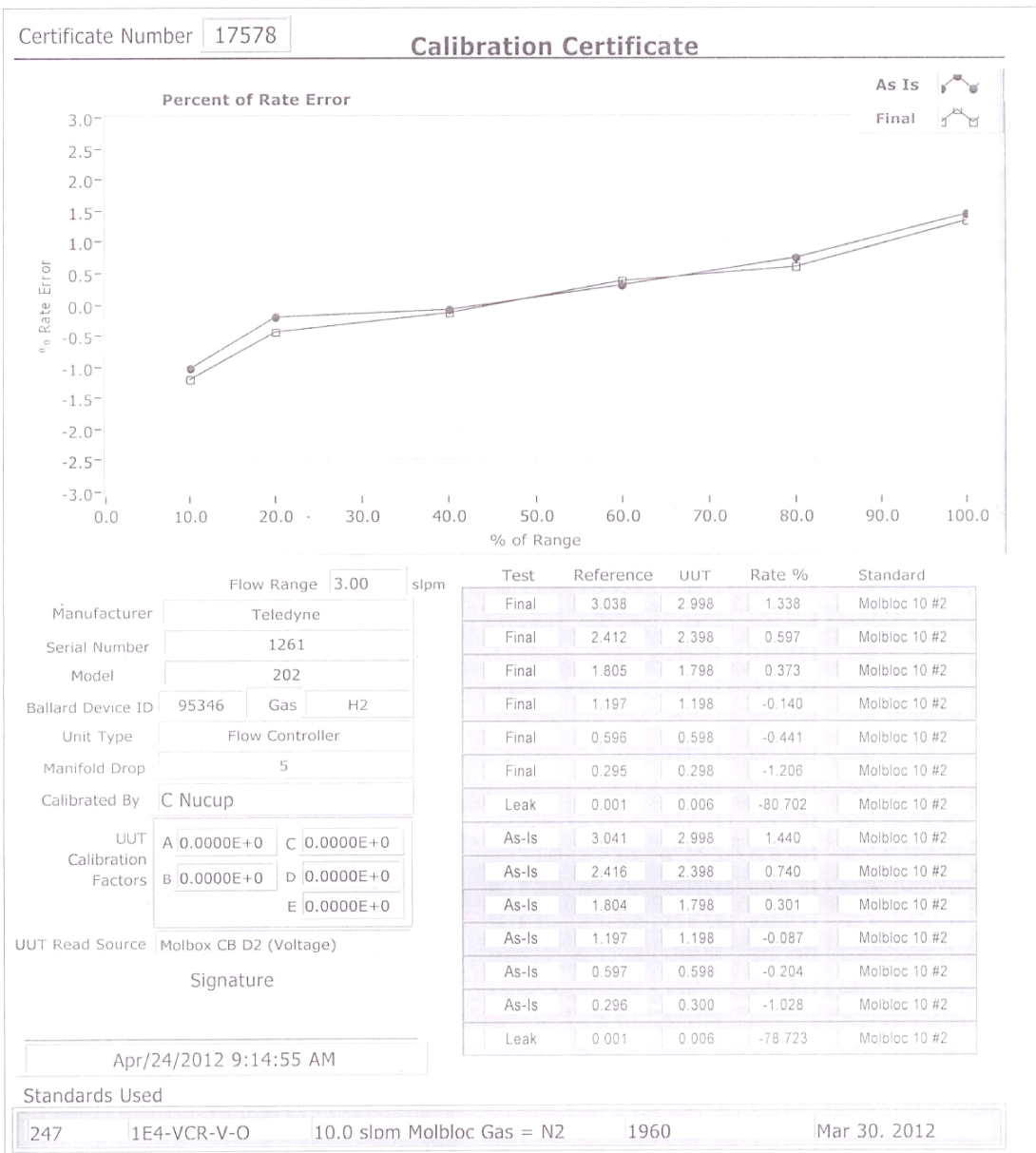### Teledyne Hastings Type 202 Hydrogen Mass Flow Controller Calibration Sheet

Appendix I.

Teledyne Hastings Type 202 Air Mass Flow Controller Calibration Sheet

Certificate Number 16951

Calibration Certificate

Percent of Rate Error

As Is / Final

% of Range

Flow Range	120.00	slpm	
Manufacturer	Teledyne		
Serial Number	123657		
Model	303		
Ballard Device ID	100074	Gas	Air
Unit Type	Flow Controller		
Manifold Drop	5		
Calibrated By	C Nucup		

UUT Calibration Factors:
A 0.0000E+0 C 0.0000E+0
B 0.0000E+0 D 0.0000E+0
E 0.0000E+0

UUT Read Source: Molbox CB D2 (Voltage)

Signature

Jun/20/2011 12:10:16 PM

Test	Reference	UUT	Rate %	Standard
As-Is	120.053	119.951	0.086	Molbloc 100 #2
As-Is	95.829	95.971	-0.148	Molbloc 100 #1
As-Is	71.989	71.966	0.032	Molbloc 100 #1
As-Is	48.124	47.956	0.350	Molbloc 100 #1
As-Is	24.058	24.006	0.215	Molbloc 100 #1
As-Is	11.922	11.980	-0.477	Molbloc 100 #1
Leak	-0.173	-0.190	-8.492	Molbloc 100 #1
Final	120.781	119.950	0.693	Molbloc 100 #2
Final	96.242	95.942	0.312	Molbloc 100 #1
Final	72.272	72.048	0.311	Molbloc 100 #1
Final	48.286	47.897	0.812	Molbloc 100 #1
Final	24.131	24.010	0.504	Molbloc 100 #1
Final	11.991	12.012	-0.173	Molbloc 100 #1
Leak	0.061	-0.122	-149.673	Molbloc 100 #1

Standards Used

251	1E5-VCR-V-O	100 slpm Molbloc Gas = N2	2053	Mar 10. 2011
128	1E5-VCR-V-O	100 slpm Molbloc Gas = N2	1849	Jan 12. 2011

Appendix J.

Comparison of the RKI sensor values with expected hydrogen concentration for each sensor

Table 8 Tests

Test	MEA	Sensor	Flow	Hydrogen Estimate	Hydrogen Measurement	Estimated Calibration
1	New	Good	0.54	3.482	3.300	0.986
			0.48	2.852	2.704	0.987
			0.40	2.134	1.965	0.958
			0.35	1.706	1.531	0.934
2	New	Partially Degraded	0.54	3.482	2.667971	0.766
			0.48	2.925	2.166506	0.741
			0.40	2.150	1.496052	0.696
			0.35	1.684	1.00957	0.599
3	New	Poor	0.54	3.434	2.708017	0.789
			0.48	2.912	2.295671	0.788
			0.40	2.109	1.743862	0.827
			0.35	1.673	1.316067	0.787
4	Leaky	Good	0.54	2.688	2.4951	0.928
			0.48	2.112	1.8409	0.872
			0.40	1.294	1.1122	0.860
			0.35	0.879	0.6961	0.792

5	Leaky	Partially Degraded	0.54	2.579	1.991	0.772
			0.48	2.070	1.606	0.776
			0.40	1.270	0.914	0.720
			0.35	0.796	0.483	0.607
6	Leaky	Poor	0.54	2.630	0.877	0.333
			0.48	2.004	0.673	0.336
			0.40	1.272	0.430	0.338
			0.35	0.799	0.277	0.346